SANDIA REPORT

SAND2017-10592
Unlimited Release
Printed September, 2017

WEC Extreme Conditions Modeling Sandia Summer Intern 2017 Report

Jarred Canning, Samuel Edwards, Tyler Esterly, Bibiana Seng, Laura Smith, William Stuart, Nevin Martin, Aubrey Eckert-Gallup, and Ryan G. Coe

Prepared by
Sandia National Laboratories
Albuquerque, New Mexico 87185 and Livermore, California 94550

Sandia National Laboratories is a multimission laboratory managed and operated by National Technology and Engineering Solutions of Sandia, LLC., a wholly owned subsidiary of Honeywell International, Inc., for the U.S. Department of Energy's National Nuclear Security Administration under contract DE-NA0003525.

Sandia National Laboratories

Issued by Sandia National Laboratories, operated for the United States Department of Energy by National Technology and Engineering Solutions of Sandia, LLC.

Available to DOE and DOE contractors from
U.S. Department of Energy
Office of Scientific and Technical Information
P.O. Box 62
Oak Ridge, TN 37831

Telephone: (865) 576-8401
Facsimile: (865) 576-5728
E-Mail: reports@adonis.osti.gov
Online ordering: http://www.osti.gov/bridge

Available to the public from
U.S. Department of Commerce
National Technical Information Service
5285 Port Royal Rd
Springfield, VA 22161

Telephone: (800) 553-6847
Facsimile: (703) 605-6900
E-Mail: orders@ntis.fedworld.gov
Online ordering: http://www.ntis.gov/help/ordermethods.asp?loc=7-4-0#online

SAND2017-10592
Unlimited Release
Printed September, 2017

WEC Extreme Conditions Modeling
Sandia Summer Intern 2017 Report

Jarred Canning
University of Texas, Austin

Samuel Edwards
University of Michigan

Tyler Esterly
University of New Mexico

Bibiana Seng
University of New Mexico

Laura Smith
Virginia Tech

William Stuart
University of New Mexico

Nevin Martin
Sandia National Laboratories
P.O. Box 5800
Albuquerque, NM 87185
nevmart@sandia.gov

Aubrey Eckert-Gallup
Sandia National Laboratories
P.O. Box 5800
Albuquerque, NM 87185
acecker@sandia.gov

Ryan G. Coe
Sandia National Laboratories
P.O. Box 5800
Albuquerque, NM 87185
rcoe@sandia.gov

Acknowledgment

This work was funded by the U.S. Department of Energy's Wind and Water Power Technologies Office. Sandia National Laboratories is a multi-mission laboratory managed and operated by National Technology and Engineering Solutions of Sandia, LLC., a wholly owned subsidiary of Honeywell International, Inc., for the U.S. Department of Energys National Nuclear Security Administration under contract DE-NA0003525.

Contents

Appendix

List of Figures

List of Tables

Preface

This report contains work completed by a group of student interns during the summer of 2017. Under the guidance of Ryan Coe, Aubrey Eckert-Gallup, and Nevin Martin, a series of interrelated projects were completed on topics relating to extreme response and survival analysis of wave energy converters (WECs). Jarred Canning studied long-term design response analysis methods for WECs. Sam Edwards studied how variation in the selection of an environmental contour affects the characterization of WEC response in extreme conditions. Sam also led the integration of various components of this report and overall editing. Tyler Esterly produced a catalog of analyses for different ocean sites. Bibiana Seng studied clustering analyses for comparing the wave environments of different ocean sites. Lori Smith performed a comparison between analyses conducted using spectral wave data and analyses using deterministic time-domain wave data. William ("Zach") Stuart studied the sensitivity and convergence of environmental contour methods.

Nomenclature

ALW All-peaks Weibull

ACER Average Conditional Exceedance Rate

cdf Cumulative Distribution Function

ECM Extreme Condition Modeling

ESSC Environmental Sea State Contour

FFT Fast Fourier Transform

H_s Significant wave height

IFORM Inverse First Order Reliability Method

ITTC International Towing Tank Conference

JONSWAP Joint North Sea Wave Project

MPM Most Probable Maximum

NDBC National Data Buoy Center

PTO Power take-off

PCA Principle Component Analysis

pdf Probability Density Function

RAO Response Amplitude Operator

RM3 Reference Model 3. A type of Wave Energy Converter.

SWIFT Surface Wave Instrument Float with Tracking

T_e Energy period

WEC Wave Energy Converter

WEC-Sim Wave Energy Converter Simulation. Part of WDRT.

WDRT WEC Design Response Toolbox `http://wec-sim.github.io/WDRT/`

Chapter 1

Introduction

Wave energy converters (WECs) are devices that use ocean waves as drivers to create electricity using a variety of methods such as hydraulics, turbines, and linear generators. The understanding and predictability of the ocean is still a major challenge and has made the development of the technology surrounding WECs difficult due to special circumstances. For example, like all marine structures, WECs must survive extreme sea states that may have not been predicted. However, unlike marine structures, WECs must generally *resonate* to harvest energy from the ocean and therefore the designers are presented with a unique challenge: how can a WEC be built in a structurally and economically efficient method such that it can be profitable and survive extreme conditions?

Presently, the method to meet this challenge, as outlined in [2] is to:

1. Represent the area of interest using hindcast simulations or buoy observations of an acceptable period, generally about 20 years;
2. Use extreme value theory and models to extrapolate to more extreme values of waves from a shorter period of record;
3. Generate environmental contours involving energy period and significant wave height to determine extreme sea states;
4. Identify one or more sea states to describe an individual or group of waves to use as an input to a numerical or physical model simulation;
5. Perform simulations or testing to predict the device response in these conditions.

Throughout this report, multiple studies on components of the design response analysis process are considered in detail. In general each of these studies utilizes the WEC Design Response Toolbox (WDRT), which is an open-source toolkit (available at http://wec-sim.github.io/WDRT/) that contains a series of Python scripts for WEC design response analysis.

First, WEC device response is considered. In Chapter 2 and Chapter 3, device responses for the different environmental contours are compared. In Chapter 4, the reliability of the

data used in the first two sections is tested by comparing National Data Buoy Collection (NDBC) buoys and Surface Wave Instrument Float with Tracking (SWIFT) buoys.

Next a series of chapters present work on the environmental characterization component of the process. In Chapter 5, an analysis of a large number of NDBC sites is conducted by utilizing clustering methods. In Chapter 6, a series of analyses are conducted to better understand the sensitivity of different environmental contour methods.

The appendix of this report includes information on computational efficiency in the WDRT and data validation.

Chapter 2

The Effect of Environmental Contour Selection on Expected Device Response

2.1 Introduction

The design of a WEC involves predicting the severity of sea states that the device may encounter throughout its operational life. WECs are unique to other ocean systems in that they are often designed to resonate; in the case of extreme sea states, this may result in potentially fatal responses due to unexpectedly violent sea states. Additionally, many current WEC designs target locations with particularly energetic seas. This is done with the hope of capturing additional energy, but also exposes the device to additional loads. To remain cost-effective, a WEC design must be sufficient to withstand loads, and undergo minimal maintenance, over a design life on the order of 25 years without unnecessary levels of over-design. Thus the problem of accurately predicting long-term loads on WEC is of utmost importance.

Currently, the practice for designing WECs (as with similar offshore structures) often involves applying numerical simulations in the nonlinear temporal domain to predict the response of the device structure to extreme sea states. WEC designers often use the following procedure [2, 3]:

1. Represent the deployment location of interest using hindcast simulations or buoy observations of an acceptable period, generally about 20 years;

2. Use extreme value theory and models to extrapolate to more extreme values from a shorter period of record;

3. Generate environmental contours of energy period and significant wave height to define extreme sea states;

4. Identify a number of sea states to create to analyze the response of the WEC (either through numerical simulation or physical experiment).

The definition of the extreme sea states is a key step in this design process. These environmental contours predict future extreme sea states based on a finite amount of existing data gathered from buoys. One way to estimate the extreme sea states is the Inverse First-Order Reliability Method (I-FORM). In the I-FORM, probability distributions are fit to each input variable which, in the case of ocean systems, are often the significant wave height and energy period. The probability fits attempts to capture the interdependency that is inherent between significant wave height and energy period [4]. These distributions are then used to predict extreme sea states and the associated probability levels with desired return periods, say 50 years, which can then be used to define a contour isoline.

The different contour methods analyzed in this study are the principal component analysis (PCA), Rosenblatt, Gaussian, Gumbel, and Clayton methods. The PCA contour method attempts to remove the correlation between significant wave height and energy period and thus better encapsulate/predict extreme significant wave height and energy period observations over extended periods [1]. The Rosenblatt method is similar to the PCA contour method, but the correlation between the significant wave height and energy period is not removed before distributions are fit [5]. The Gaussian, Gumbel, and Clayton methods are known as copula methods. In a copula method, the relationship between the significant wave height and energy period is predefined by certain parametric correlations (see, e.g. [5]). It follows that the shapes of the copula contours are generally rigid with respect to the given sample data.

It should be noted that the "contour approach" ignores short-term variability in the interest of efficiency [6]. Often, correction factors are applied to the short-term results in order to account for short-term variability and determine the long-term extreme (see, e.g., [7] and [8]). However, these correction factors are known to be specific not only to the device type, but also the response of interest (e.g., mooring tension versus power take-off (PTO) load).

Step 4 in this design process involves the prediction of WEC responses based on the previously determined set of sea states. This step is often carried out using some combination of numerical models and experimental testing. As outlined in [9], while numerical codes such as WEC-Sim and WaveDyn are often unable to predict loading and device response on the most extreme waves, they are generally able to capture accurate trends in extreme response.

For this WEC design approach to be accurate, it follows intuitively that the environmental contour must also be accurate. However, with a large range of environmental contours to choose from, choosing the best contour (that which neither under- or over-predicts extreme waves) is not always straightforward. It is also unclear just how influential the accuracy of an environmental contour will be on predicting extreme loads for a WEC. This study aims to compare a wide range of available contour methods. Beyond a comparison of the contour predictions, we also seek to determine the difference in WEC response when using different contour methods, and therefore begin to assess the importance of choosing an accurate contour method and provide some guidance on the relative performance of various contour methods.

To accomplish this, the previously described methods are used to produce environmental contours for a chosen individual site. These contours are compared to each other and with respect to the underlying data. In order to understand the repercussions to WEC design, each contour is then used to perform a design analysis on a single WEC device. The results of these analyses are then compared to give insight into the range of results and the sensitivity of the design process to the different contours.

2.2 Methods

For this study, the Reference Model 3 (RM3) device was chosen for analysis [10]. To perform the analysis, spectral data from NDBC Buoy 46022, which was considered the deployment location for the RM3, over the years 1996-2016 were used to generate PCA, Rosenblatt, Gaussian, Gumbel, and Clayton contours. The contours were calculated using features within the WEC Design Response Toolbox (WDRT) [11]. The WDRT is a set of Python codes with the functionality to generate environmental contours from a set of wave spectral density observations. As per guidance in [3], a return period of 50 years and a sea state duration of three hours were chosen. Figure 2.1 shows the NDBC data along with the five contours. Six energy periods were chosen to define extreme sea states along each of the contours. The following energy periods were chosen for analysis: 7.00, 9.88, 12.76, 15.64, 18.52, and 21.40 seconds. These sea states are shown in Figure 2.1 and listed in Table 2.1.

WEC-Sim simulations [12] were performed to find the heave power take-off (PTO) force of RM3 in the selected sea states from the different contour methods. The significant wave height (H_s) and energy period (T_e) pairs for each contour method, were used to perform a WEC-Sim simulation. Here, JONSWAP spectra with the default peak enhancement factor of 3.3 were generated from each H_s-T_e pair. The WEC-Sim application simulates the response of a WEC using a 3-D model built in Simulink and an input wave spectrum.

To ensure that the results were realistic, the PTO damping coefficient was calculated to maximize the power output. The method utilized by Falnes [13] was used to select

Table 2.1: Significant wave height values from each contour method.

T_e, s	PCA H_s, m	Rosenblatt H_s, m	Gaussian H_s, m	Gumbel H_s, m	Clayton H_s, m
7.00	5.21	5.44	6.72	6.93	7.49
9.88	7.66	6.96	7.84	7.51	8.20
12.76	9.68	8.05	8.18	7.76	7.95
15.64	10.94	7.96	8.11	7.94	7.30
18.52	11.04	6.89	7.69	8.10	6.41
21.40	9.23	4.24	6.79	8.20	5.15

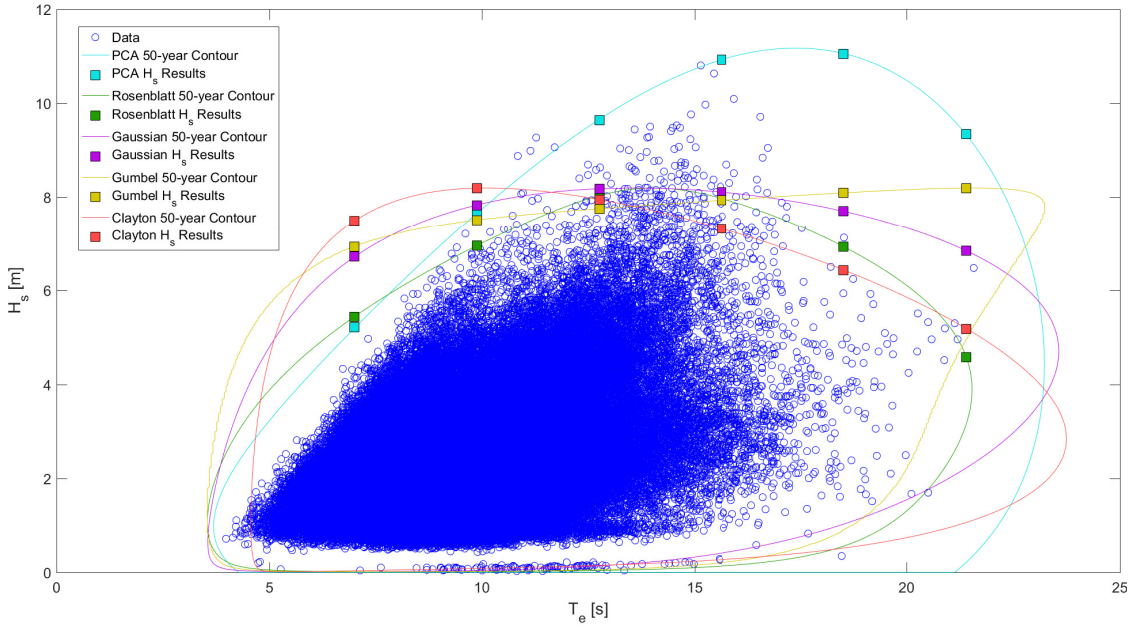

Figure 2.1: All contours with data from NDBC Buoy 46022 as well as energy period choices for analysis.

the optimal damping coefficient for each energy period. It should be noted that the spring stiffness value for the PTO was chosen to be zero for simplicity. The device response, namely the PTO force, was output from WEC-Sim in the form of three-hour time series. The PTO force was selected because it is a major driver in the design of the WEC and more specifically the power take off device [14].

2.2.1 Short-term Extremes

From each WEC-Sim time series, a statistical short-term extreme was predicted. Three major methods were applied to predict short-term extremes: most-probable maximum (MPM), all-peaks Weibull (APW), and Average Conditional Exceedance Rate Method (ACER).

Most-probable Maximum - Rayleigh

The most probable maximum is, as specified by the name, the most likely maximum value in the exposure period and not necessarily the mean or median value. From a probabilistic stand point, if an array of 100 WECs each underwent the same three-hour wave set and if interactions between the arrayed WECs could be ignored, the most probable maximum value would be the most frequent maximum response experienced by the WECs. The most probable maximum method was considered here because it makes use of the entire time series by shifting it into the frequency domain.

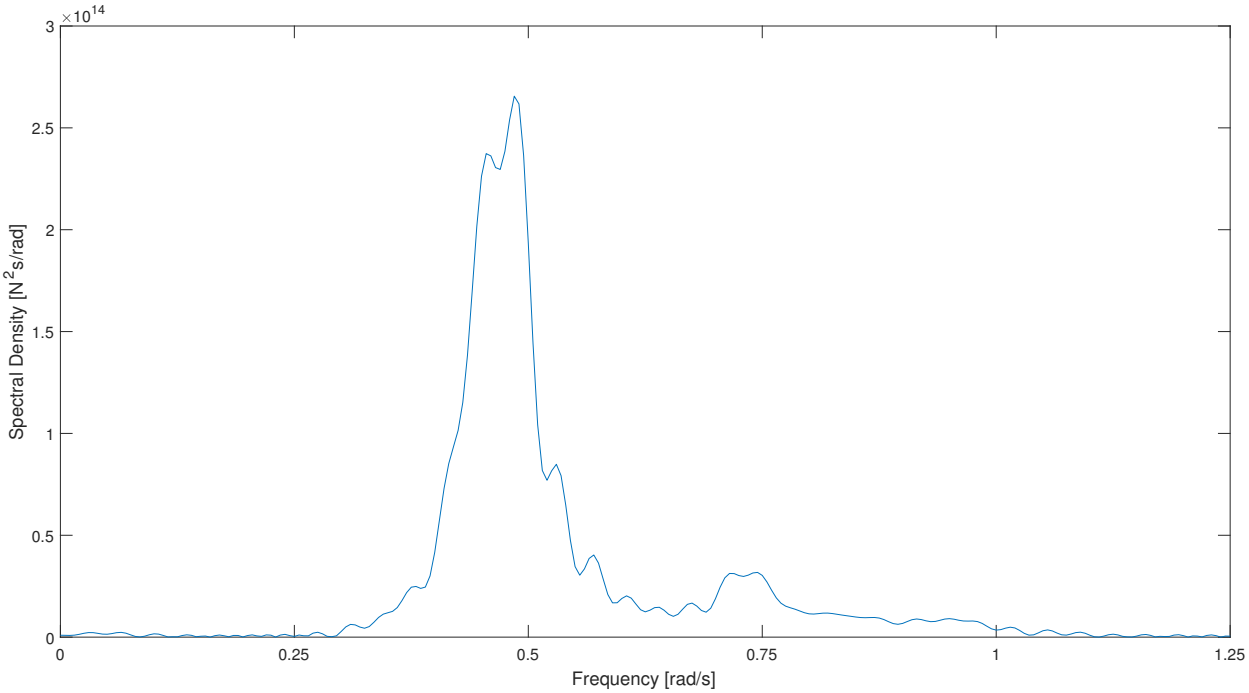

Figure 2.2: Spectral density function for the PTO force time series from the PCA contour method with an energy period of 12.76 seconds.

To determine the MPM, each time series must be converted into the frequency domain. To do so, the Wiener-Khintchine theorem [15] is used to transition from the temporal domain to the frequency domain. From the time series, autocorrelation functions were formed so that the response spectra could be found.

$$R(\tau) = \int_{-T/2}^{T/2} \zeta(t)\zeta(t+\tau)\, dt \tag{2.1}$$

$$S(\omega) = \int_{-\infty}^{\infty} R(\tau) e^{-i\omega\tau}\, d\tau \tag{2.2}$$

Here, $R(\tau)$ is the autocorrelation function calculated on the time lag τ. This is evaluated for time series data, ζ, with a known length of record, T. Applying (2.2), the frequency-dependent spectral density function, $S(\omega)$ can be obtained [16].

Figure 2.2 shows an example of a one-sided response spectra formed from a PTO force time series. Using the spectral density functions, the MPM for each response over the three

hour sea state was determined as [17]

$$\zeta_{3hr} = \sqrt{2m_0 \cdot \ln(\frac{T_E}{T_0})(1 - \frac{\epsilon^2}{2})}$$

where:

$$\begin{aligned} \zeta_{3hr}: &\quad \text{Most probable maximum value in three hours} \\ m_n: &\quad \text{n}^{th} \text{ moment of the response spectrum} \\ T_E: &\quad \text{Exposure period or duration of sea state, seconds} \\ T_0: &\quad \text{Average period or } 2\pi\frac{m0}{m1}\text{, seconds} \\ \epsilon: &\quad \text{Bandwidth parameter or } \sqrt{(1 - \frac{m_2^2}{m_0 m_4})}. \end{aligned} \tag{2.3}$$

The bandwidth parameter is a measure of the narrow-bandedness of the process; when the bandwidth parameter is equal to zero, it is very narrow banded. Generally, the assumption that the process is narrow banded is made, especially with a Joint North Sea Wave Project (JONSWAP) wave spectrum as the input (see, e.g., [18]). However, the additional term in the most probable maximum definition was included for precision. Coupled with the definition of MPM are the following assumptions of the response: it has a zero-mean and it is stationary and ergodic. It should be noted that (2.3) is derived from the assumption that the peak distribution is a Rayleigh distribution. While it is true that an ideal wave spectrum will have a Rayleigh amplitude distribution, it may not be the case for a response such as the PTO force due to additional interactions with other components within the power conversion chain. As such, other methods to approximate short-term extremes were explored to improve upon potentially invalid assumptions made in the Rayleigh MPM method.

All-peaks Weibull

An alternative method is the all-peaks Weibull method [19]. In this method, a Weibull distribution is fit to the local maxima between upcrossings and the CDF is determined.

$$F(z) = 1 - e^{-(\frac{z}{\alpha})^{\lambda}} \tag{2.4}$$

$$F_e(z) = F(z)^q$$

where:

$$\begin{aligned} F(z): &\quad \text{Weibull CDF} \\ \alpha: &\quad \text{Scale parameter} \\ \lambda: &\quad \text{Shape parameter} \\ F_e(z): &\quad \text{Extreme CDF} \\ q: &\quad \text{Number of peaks in exposure period (3 hrs)} \end{aligned} \tag{2.5}$$

For a Weibull distribution, (2.4) is used. To determine the extreme distribution from the peak distribution, (2.5) is used. After the extreme CDF was determined for each time series, it was differentiated to obtain the extreme PDF. Then, the peak value from the PDF was found and compared to the MPM values.

Note that the APW is similar to a Weibull variation on the MPM method. Using the exposure period of three hours and average period, which can be calculated using the response spectrum, to determine the amount of events in the period, the minimum expected maximum value in the exposure period is determined by solving for $\tilde{\zeta}_{1/N}$ in (2.6).

$$\frac{1}{N} = \int_{\tilde{\zeta}_{1/N}}^{\infty} P_{\tilde{\zeta}}(z)\, dz \tag{2.6}$$

The minimum expected maximum value in N events, $\tilde{\zeta}_{1/N}$, effectively becomes the lower bound in a distribution that is similar to an APW Extreme PDF when considering the relative probability of the minimum expected maximum value to loads that are larger. The centroid of the area beginning at $\tilde{\zeta}_{1/N}$ and ending at infinity is the most probable maximum, and also the peak value of the extreme PDF.

Average Conditional Exceedance Rate Method

The last method compared considered here is the Average Conditional Exceedance Rate (ACER) method [20]. In the ACER method, the number of exceedances of some threshold is measured for different conditions related to the number of preceding non-exceedances. Ultimately, at least for the purpose of this paper, ACER can be used to determine a "predicted T-years return level estimate" to estimate an extreme value over the time period of "T-years". For this study, the "T-years" was set to 3-hours so that it could be compared to the methods listed above.

2.3 Results

The following two sections present environmental comparison results. First, the 50-year environmental contours produced from the NDBC 46022 data are compared directly to each other. Next, a comparison of short-term extreme response methods is conducted to down-select to a single method for determining a characteristic 3-hour extreme response from a time series. Finally, the results of WEC response analyses using each contour are considered and compared in order to understand the WEC design repercussions for choosing between environmental contours.

2.3.1 Comparison of Contours

As discussed in the Introduction section, environmental contours must predict the envelope of sea states likely to occur in some return period, which is often longer than the period of record. A good environmental contour should neither over- or under-predict the bounds of this envelope, as this could result in costly over-design or failure respectively. Any time a sea state occurs outside of a contour, a WEC could undergo more severe conditions than it was designed for and be damaged or destroyed.

One concern, and a metric that can be used to assess performance among contour methods, is the "exceedance" of a contour. For example, if 20 years of observations exist and a 50-year contour is desired, the 50-year contour is exceeded by an amount of observations from the 20 years of data. This occurrence is generally unavoidable and it is desired that a very small percentage of sample observations exceed a contour expected to encapsulate more years than were sampled. From Figure 2.1, it can be observed that the PCA contour method is a viable option and may be exceeded by gathered data less than alternative parametric contour methods such as the Rosenblatt, Gaussian, Gumbel, or Clayton methods.

To determine the quality of the contours generated for NDBC Buoy 46022, the number of contour exceedances were tabulated for two different energy period ranges: $10.0 < T_e < 17.5\,\text{s}$ and $T_e > 17.5\,\text{s}$. The exceedances were split up into these two energy period ranges because it highlights two distinct trends in the exceedances: (1) the PCA method predicts extreme significant wave heights in the energy period range of $10.0 < T_e < 17.5\,\text{s}$ well compared to the other four methods; (2) the PCA method (and even the Gumbel method) is more conservative in extreme significant wave height estimation than the other contours for $T_e > 17.5\,\text{s}$. Table 2.2 lists the number of sample exceedances of each contour for both aforementioned energy period ranges.

As mentioned, the PCA and Gumbel methods conservatively estimate extreme waves at larger energy periods (only 5 total exceedances of all contours occur for $T_e > 17.5\,\text{s}$). It follows that the relatively large estimates made by the Gumbel and PCA methods may result in structural over-design, potentially resulting in a WEC that is not economically viable. On the contrary, in the energy period range of $10.0 < T_e < 17.5\,\text{s}$, which will likely result in the most severe results due to the proximity to the breaking wave line, the PCA contour method

Table 2.2: Number of observations each contour was exceeded (for H_s larger than 0.3 m) for specified ranges of energy periods.

Energy Period Range [s]	PCA Exceedances	Rosenblatt Exceedances	Gaussian Exceedances	Gumbel Exceedances	Clayton Exceedances
10.0-17.5	5	91	73	127	160
> 17.5	0	3	0	0	2

Table 2.3: Maximum PTO force value extracted from each time series, MPM using a Rayleigh distribution, MPM using a Weibull distribution, Weibull All-Peaks method, and ACER averaged for each energy period.

T_e, s	Time Series Maximum	Rayleigh MPM	Weibull MPM	APW	ACER
7.00	5.39	4.98	5.24	5.64	5.83
9.88	13.68	12.37	13.46	14.56	14.24
12.76	20.99	16.94	20.32	20.85	21.22
15.64	14.53	13.30	14.12	15.48	15.48
18.52	10.88	10.54	11.43	11.59	11.78
21.40	6.51	7.41	7.27	8.43	8.34

is only exceeded 5 times while the other contours are exceeded an average of 113 times. It should be reiterated that the samples provided were from only 20 years of data, and the contours are meant to predict 50 year extreme waves. That said, the amount of exceedances of the Rosenblatt, Gaussian, Gumbel, and Clayton methods are unacceptable.

2.3.2 Short-term Extreme Comparison

Before comparing the short-term extreme responses resulting from various contours, a comparison of the short-term extreme response prediction methods discussed in Section 2.2.1 was considered.

Table 2.3 shows the average maximum value extracted from each time series, MPM, the APW, and ACER methods for the PTO force. Initially, it is noted that with a Rayleigh distribution, the MPM will be exceeded 60.7% of the time [16] in the exposure period. When comparing the Rayleigh MPM values predicted in the exposure period of three hours with the maximum values from the three hour time series, it was found that the maximum values from the time series were larger than the most probable maximum 60% of the time. Given more time series, it is likely that this percentage would tend towards the expected 60.7%. While the Rayleigh MPM seemed initially valid, it was noted that when it did under predict the time series maximum, it was generally by a relatively large margin. By extension, the Rayleigh MPM was generally lower than the other short-term extreme methods as well. On

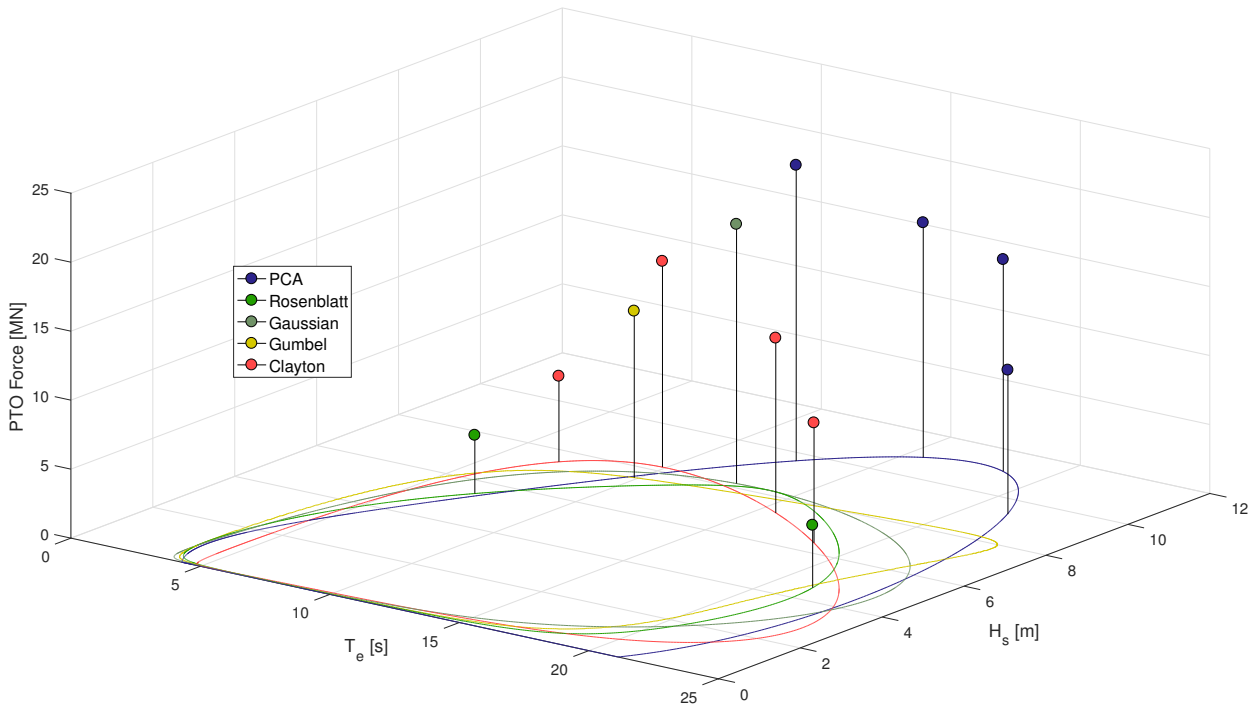

Figure 2.3: Extreme PTO force response for each contour method at given energy periods.

average, the Rayleigh MPM yielded results about 5% lower than the APW, 10% lower than the Weibull MPM, and 20% lower than the ACER method.

Based on this comparison of short-term extreme methods, the APW method was used to compare extreme responses resulting from each contour. The APW followed the time series maximum relatively well and, unlike the Rayleigh MPM, the peak distribution was separately fit for each time series to remove any uncertainties regarding the peak distribution of the response instead of enforcing the parameters. The minimum, maximum, and average MPM response for each energy period is shown in Figure 2.3, the response of each contour method and energy period is shown in Table 2.4, and the coefficient of variation at each energy period is visualized in Figure 2.4.

2.3.3 WEC Extreme Response Comparison

Figure 2.3 shows extreme PTO force predicted from each contour method. Table 2.4 lists these results along with the coefficient of variation and, average extreme PTO force for each energy period. To illustrate the divergence in design, at an energy period of 21.4 s, the PCA method predicted a extreme PTO force of 10.45 MN while the Rosenblatt method predicted an extreme PTO force of 4.54 MN. Clearly, even after safety factors are considered, the structure required based off of these two methods would vastly differ.

Generally, the PCA contour method produced the largest extreme PTO forces, as the method predicts larger significant wave heights than the other methods at energy periods

Table 2.4: Coefficient of variation, average of the extreme PTO force for each energy period, and response of each contour.

T_e, s	Coefficient of Variation [ ]	Average [MN]	PCA [MN]	Rosenblatt [MN]	Gaussian [MN]	Gumbel [MN]	Clayton [MN]
7.00	0.16	5.24	4.52	4.23	5.36	5.87	6.21
9.88	0.08	13.46	12.64	13.85	13.82	12.058	14.92
12.76	0.05	20.32	21.44	19.96	18.79	20.57	20.86
15.64	0.12	14.12	17.02	13.36	13.35	14.19	12.69
18.52	0.21	11.43	15.37	11.00	10.92	11.18	8.71
21.40	0.32	7.27	10.45	4.54	8.25	7.68	5.46

above about 11 seconds (which includes the resonant $T_e = 12.76\,\text{s}$ sea state where extreme PTO forces were predicted to be largest).

It can be noted that the PTO force is correlated with the significant wave height (H_s). Upon investigation, the correlation coefficient between the two was calculated to be 0.67.

While not directly correlated, it is clear that a relationship exists between PTO force and significant wave height (H_s) as shown by Figure 2.5. Since the RM3 system is mostly linear, this relationship between input and output is expected. Given the dependence of the PTO force on significant wave height, it follows that the coefficient of variation increases as the variation in significant wave height (H_s) at a given energy period (T_e) amongst the contour methods increases. In other words, since the contour methods have height predictions diverge at larger energy periods, the PTO force predictions should, and do, follow a similar trend (see Table 2.4). This increasing coefficient of variation marks divergence in design decisions regarding contour selection.

However, looking at the relationship between PTO force and energy period, we can see from Table 2.4 that the PTO force peaks for the sea state with $T_e = 12.76\,\text{s}$. This peaked resonant behavior is expected for the resistant damping control applied here. This sea state would effectively control the maximum loading design for the PTO in this scenario. While the PCA contour leads to the largest extreme PTO forces at this energy period, the other contours are not substantially different. This is not surprising, as this energy period coincides with the lowest variation in significant wave heights predicted by the contours (see Figure 2.4). This is really a fortunate coincidence, in that because the controlling sea state for extreme PTO loading of the RM3 occurs where the contours mostly agree, the choice in contour matters little when considering the extreme PTO loading for this device.

However, is should be noted that this region of the contours showed the largest number of exceedances. Referring back to the Comparison of Contours section, it is also interesting to note that, the majority of contour exceedances occur for $10.0 < T_e < 17.5\,\text{s}$ for the other contours (see Figure 2.1 and Table 2.2). On average, the Rosenblatt, Gaussian, Gumbel, and Clayton methods are exceeded 113 times while the PCA contour is only exceeded 5 times in this range of energy periods. Thus, while the differences in extreme PTO force

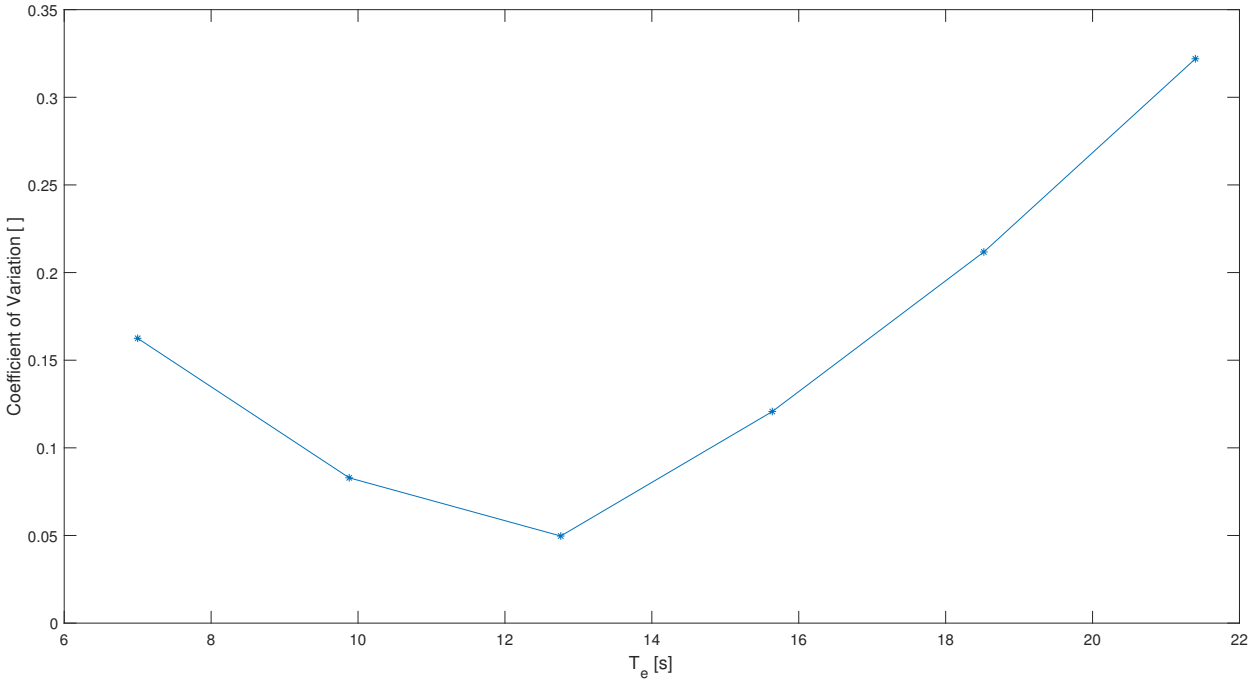

Figure 2.4: PTO extreme response prediction coefficient of variation amongst contour methods for a range of sea state energy periods.

produced from the different contours were shown to be relatively small in this case study, the possibility of larger than expected waves in this region should encourage a designer to use conservative factors of safety.

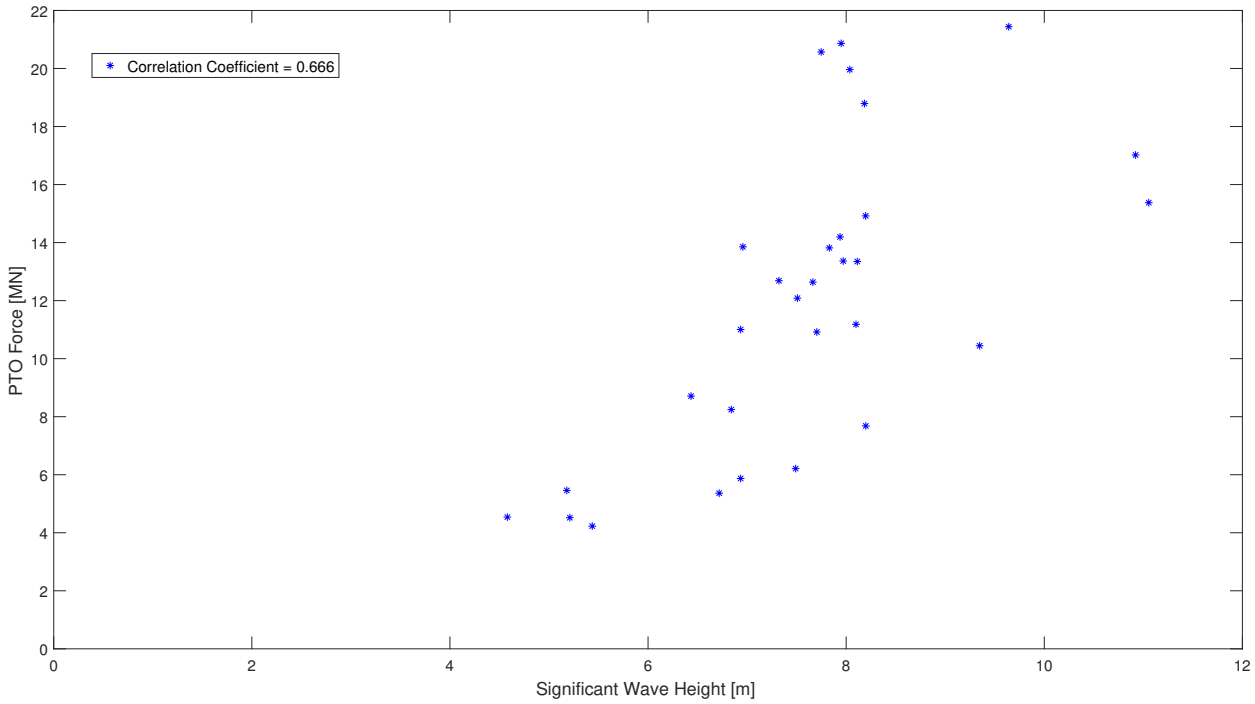

Figure 2.5: Relationship between significant wave height and PTO force.

2.4 Discussion and Conclusion

The design of a WEC requires precision as well as forbearance - it is a difficult prospect to design the most cost effective structure while attempting to provide it with the strength to survive extreme sea states that may not have been predicted over a 25-year operational life, especially when there is a limited period of record for observations made by buoys. As such, the choice in contour method used for preliminary design seems to be an important step. As shown in the analysis, the choice does have consequences - especially for longer energy periods - where the variation in significant wave height predictions for each contour method begin to separate the expected responses. However, for some responses of interest, such as the extreme PTO force in this case, the choice of a contour method may be less important than other factors. While only a single site and set of observations was analyzed, it can be concluded that the variance in expected response from the different contour methods is considerable, especially at longer energy periods, and that it is difficult choose a single contour method that optimizes survivability and cost effectiveness.

Observing NDBC Buoy 46022 (See Figure 2.1 and Table 2.2), it can be seen that most contour exceedances occur between energy periods of 10.0 and 17.5 s. Given these exceedances, one would expect that the contour method that is least exceeded would be selected. In this specific case, the PCA method would be selected. However, the coefficients of variation of the PTO force at these energy periods do not completely portray the exceedances. That is to say, while the PCA method is exceeded much less than the other methods, there was relatively low variation in the predictions of extreme significant wave height and therefore

extreme PTO force. As would be the case for many WECs, this is the region where resonance, and therefore the largest PTO loads under a resistive control strategy occur. This is a somewhat fortunate result, meaning that, at least when considering the maximum load for a PTO, contour selection may not be as important as other factors. Thus, while it seems that the other contours provide similar predictions for extreme PTO force in the RM3, a designer might select the PCA curve and then feel more comfortable with a lower factor of safety given the lower rate of exceedances.

It can also be noted at the longer energy periods, less contour exceedances occur (See Figure 2.1 and Table 2.2). At the longer energy periods, the PCA method predicts considerably larger significant wave heights than the other contour methods. It follows that the PCA method predicts larger PTO forces at these longer energy periods, even given the rarity of observed waves approaching the limits of the contour. However, since these waves are at frequencies above resonance, the extreme PTO load response analyzed here was always lower than those predicted at resonance. For a response, such as mooring tension, which is driven by low-frequency phenomena, the relative performance of the contour methods in this region would result in vastly different in design decisions.

In future work, it should also be considered that the device may enter "survival mode" when the waves reach a certain height. Again, this was not accounted for in the analysis for simplicity. It is true that forces may not reach the values shown in the analysis in the following sections, but it can be said that the comparison between the responses from the contour methods at the given energy periods is still valid.

Additionally, further study should consider a wider range of WEC responses. Other response of interest may include structural loads, mooring line tension, and PTO extensions (i.e., for end-stops). Along with this, it will also be necessary to consider a wide range of locations. The location assessed here has unique environmental characteristics, thus the results may be quite different when considering a site, e.g., off the coast of Hawaii or Alaska.

Chapter 3

Long-term Response Analysis

As stated in Chapter 2, violent environmental conditions play a key role in the design and operation of a WEC. To produce maximum power, a WEC must be able to safely operate under the conditions present at its deployment site. As such, reliability analyses based on extreme sea state simulations are critical in assessing the performance and design life of a WEC [21].

This section covers the processes and methods used to determine the 50-year load extremes for different response values of RM3. Simulations are run for each desired sea state on RM3 using WEC-Sim. Two methods are considered for estimating the 50-year load extremes. The first method uses statistical extrapolation to fit a distribution for quantiles of interest. Then, probabilistic predictions of long-term conditions can be estimated by integrating over the applicable sea states. This process is know as direct integration of the sea states and is considered a "brute force" method for obtaining the long-term loads. The second method uses IFORM and environmental contours to determine a targeted return period design. Both of these methods have been employed in the extrapolation of extreme wind turbine loads [22, 23]. The two methods are explained in more detail in the following pages. Once the long-term responses are determined for each method, comparisons are made in terms of efficiency and associated errors.

In this study, we will investigate the heave and surge forces on the PTO as well as the stroke length. All three of these responses provide some insight to the power production or operational reliability of RM3. For example, RM3 primarily generates power via the heave velocity of its float [24]. As such, we should consider the heave force on the PTO as one of the quantities of interest in order to provide a meaningful analysis. Similarly, we will also examine the stroke length (PTO extension) because the mechanical design of the PTO must be sufficient to accommodate the largest expected displacements. The surge force on the PTO equates to a bearing restraint force that deals with the structural quality of the WEC, so it is also a quantity of interest. Figure 3.1 details the directions of each response for RM3. Note that the stroke length and heave force are in the same direction.

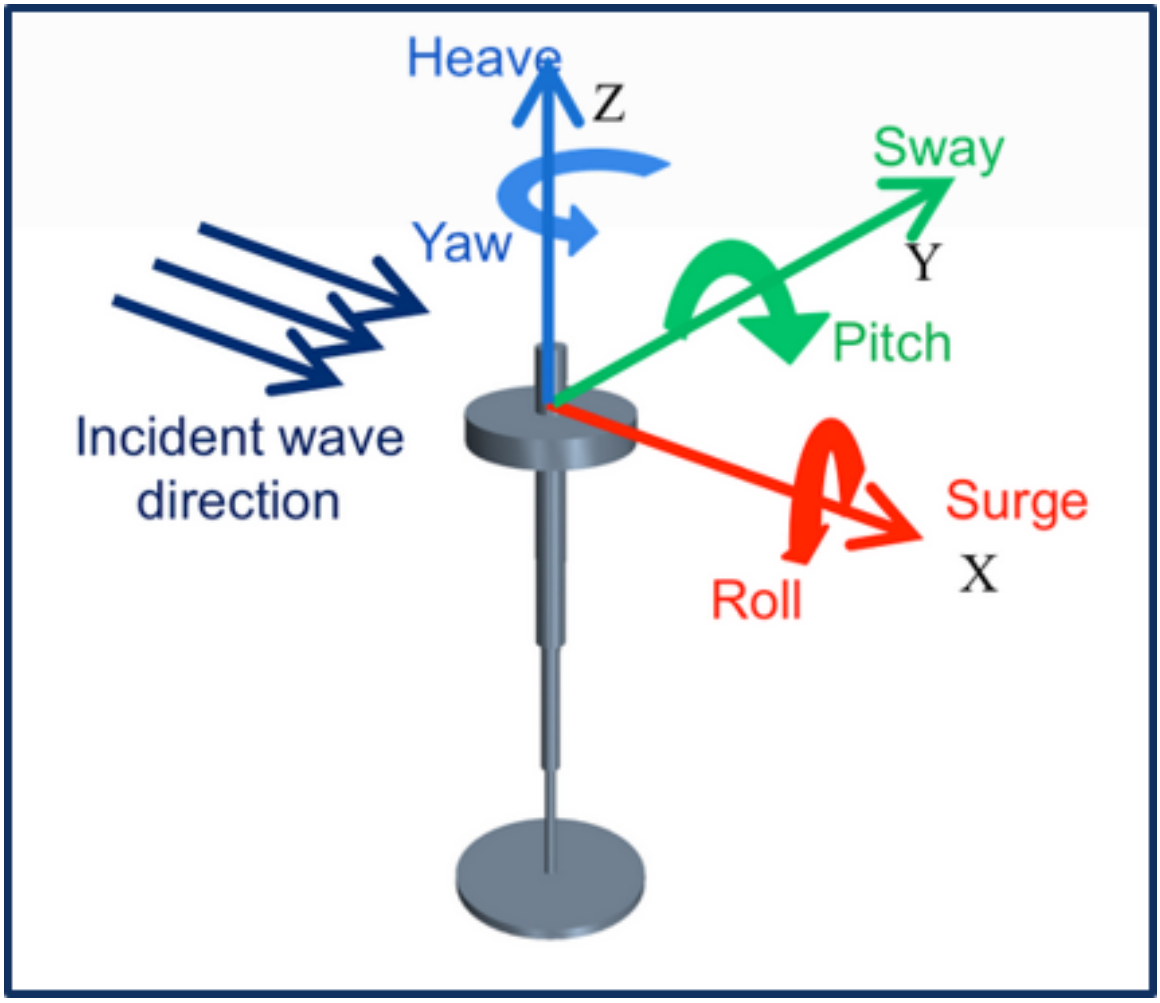

Figure 3.1: Degrees of freedom for RM3.

3.1 Direct Integration

Due to the highly variable nature of the seas, it is important to calculate accurate long-term responses for a variety of different return periods. As a result, full integration of the sea states is often used to predict low probability loads that a structure could face [22]. Direct integration weights the short-term extreme loads with the sea state likelihood and then integrates over all environmental conditions, as shown in (3.1).

$$P_T = P[L > l_T] = \int_X P[L > l_T | X = x] f_X(x)\, dx \tag{3.1}$$

Here, P_T is the long-term exceedance probability. Long-term load is given by l_T and $f_X(x)$ is the joint probability density function of the environmental conditions The short-term extreme distribution is $P[L > l_T | X = x]$. The load and sea state random variables are L and X respectively.

Here, one can change the value of l_T until a target exceedance probability is met. As a result, the process to find long-term loads using direct integration is often iterative. Conversely, one can also systematically change l_T to gain the full long-term distribution of a WEC system and then read off the response value that corresponds to the exceedance probability. Since we are concerned with the 50-year load extremes, the exceedance probability using 1-hour response extremes is equal to $1/(50 \times 365.25 \times 24)$ or 2.28×10^{-6}. It is important to note that (3.1) is actually an approximation of the full integration formulation. The exact equation is given in (3.2) [25]:

$$P_T = exp\left(\int_X log(P[L > l_T|X = x]) f_X(x)\, dx\right) \tag{3.2}$$

where *log* refers to the natural logarithm. In practice, there is often very little difference between the output values from the above formulations. Therefore, we will use (3.1) for the remainder of this study.

The direct integration method, while accepted as the exact value, is computationally expensive as it integration over all environmental conditions. It is computationally impractical to simulate WEC response for all sea states (1996-2016). Instead, we have devised a binning scheme to cut down on the simulation effort while still covering the entire sea state domain. Figure 3.2 shows the bin division that was considered for this study.

In this figure, the sea state space is divided into 30 discrete bins. Bins were defined by equally spacing the significant wave height axis by 1.5 meters and the peak period axis by 3 seconds. A random sea state within each bin is selected as the representative sea state of that bin and simulations will be run based on its environmental parameters. The weight of each bin is the number of points that lie within that bin divided by the total number of applicable sea states. For reference, the 50-year contour determined by the PCA method is also shown. Note that some sea states are not included in any of the bins; this is because a minimum tolerance was established for the binning scheme. If a bin did not contain at least 20 sea states, then it was deemed insignificant and no simulations were conducted in its space. Once the bin weights and representative sea states are determined, WEC-Sim is used to run 15 separate 1-hour simulations per bin. A block maxima approach is used to extract the extreme data for each bin from each of the 15 simulations. The extreme data is then fit to a Weibull distribution (refer to (2.4)) which serves as the short-term extreme distribution. Using the bin weights and short-term extreme distributions, one can iterate l_T in (3.1) until the target exceedance probability for 50-years is achieved.

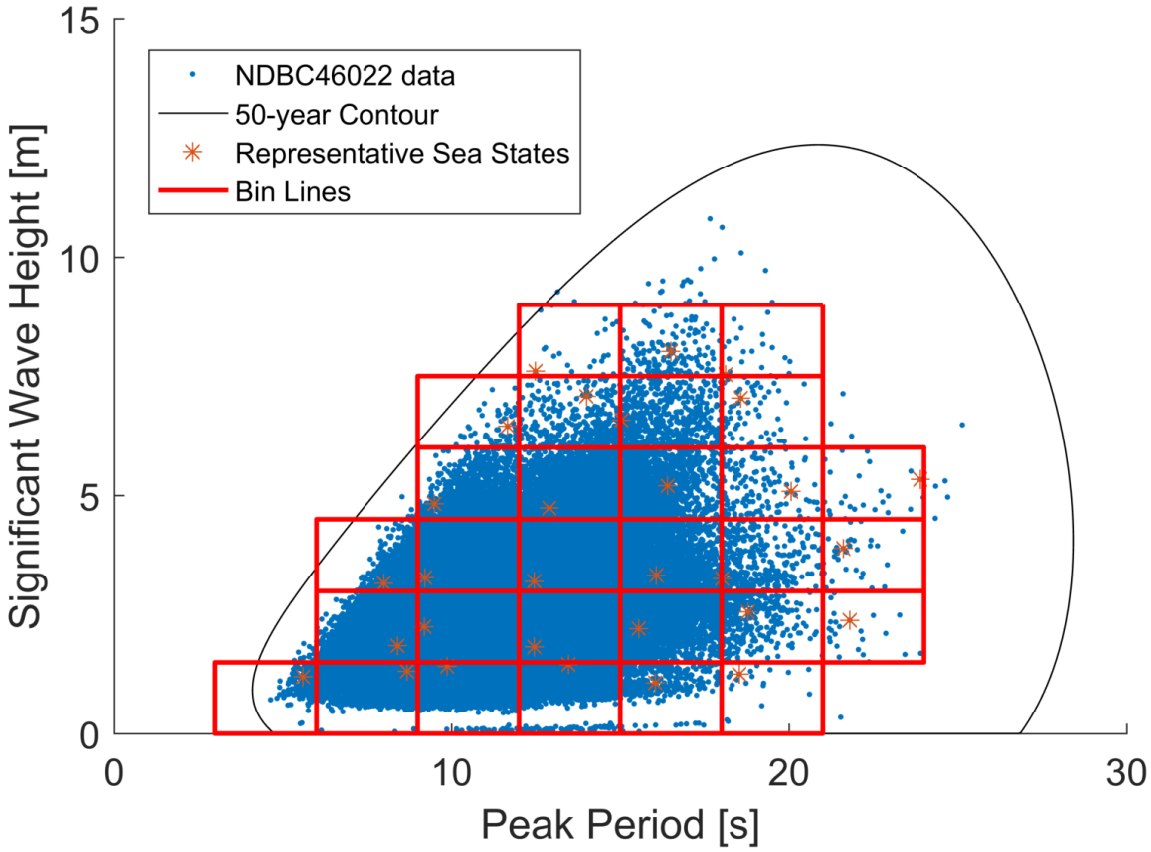

Figure 3.2: Binning scheme and representative sea states for NDBC 46022.

3.2 Environmental Contour Method

While direct integration of the sea states is an expensive process, an alternative method is to use the 50-year contour to find the long-term loads. This method, known as the environmental contour method, searches along an environmental contour for the largest median response value. Because there is no fitting or integration over the sea state space, the environmental contour method is more efficient than direct integration. However, only median values are compared to determine a rare load fractile, which means that response variability is neglected and the method is not as accurate as integration of the sea states. There is a way to correct the environmental contour loads [22], but that strategy was not used in this study.

We begin by constructing the 50-year contour using the PCA method [26] and selecting 20 sea states along its length. The selection of the sea states was not random; we concentrated the points near the breaking wave line (i.e. higher significant wave heights and smaller peak period values) because we noticed higher response values near this boundary. Figure 3.3 shows the median-level response surfaces from the direct integration analysis for each of the quantities of interest. These response surfaces show that higher median values occur with higher significant wave heights and smaller peak periods. Additionally, Figure 3.4 displays

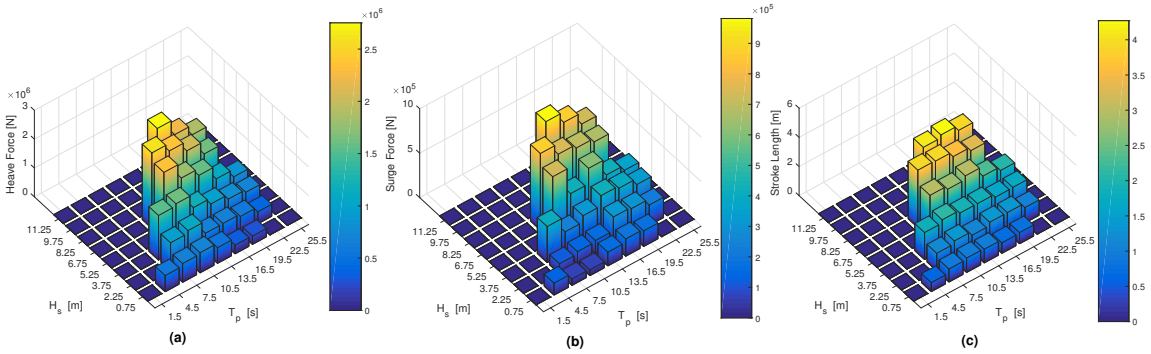

Figure 3.3: Median response values for each bin for (a) heave force, (b) surge force, and (c) stroke length.

the selected sea states along the 50-year contour for this study.

Again, 15 separate 1-hour simulations are run for each sea state and the block maxima method is used to extract load extremes. Here, we pick the median value from each sea state and search for the largest value, which is our design load l_T. Figure 3.5 displays the median responses for each sea state along the contour.

As one can see, the highest loads for all responses seem to occur near the breaking wave line. Heave force and stroke length appear to have a gradual increase to a maximum value in the middle of the selected sea states. Surge force reaches a maximum at a lower significant wave height followed by a mixture of responses, which could indicate that surge is highly variable in this range of sea states.

Another analytical method that is commonly used is three-dimensional IFORM, or 3-D IFORM for short [22], [23]. This method works by establishing the full probability distribution for the extreme load (which would be L in (3.1)) and searching for a maximum response on a different load fractile using some reliability index, β_T. The reliability index is directly related to the desired exceedance probability, P_T. For comparison, the environmental contour method applies the same principles but only searches along the median fractile level. In effect, we can call the contour method two-dimensional IFORM, or 2-D IFORM. Although more accurate than the environmental contour method, 3-D IFORM requires much more computational effort and statistical fitting methods. As a result, we have not included 3-D IFORM in this study.

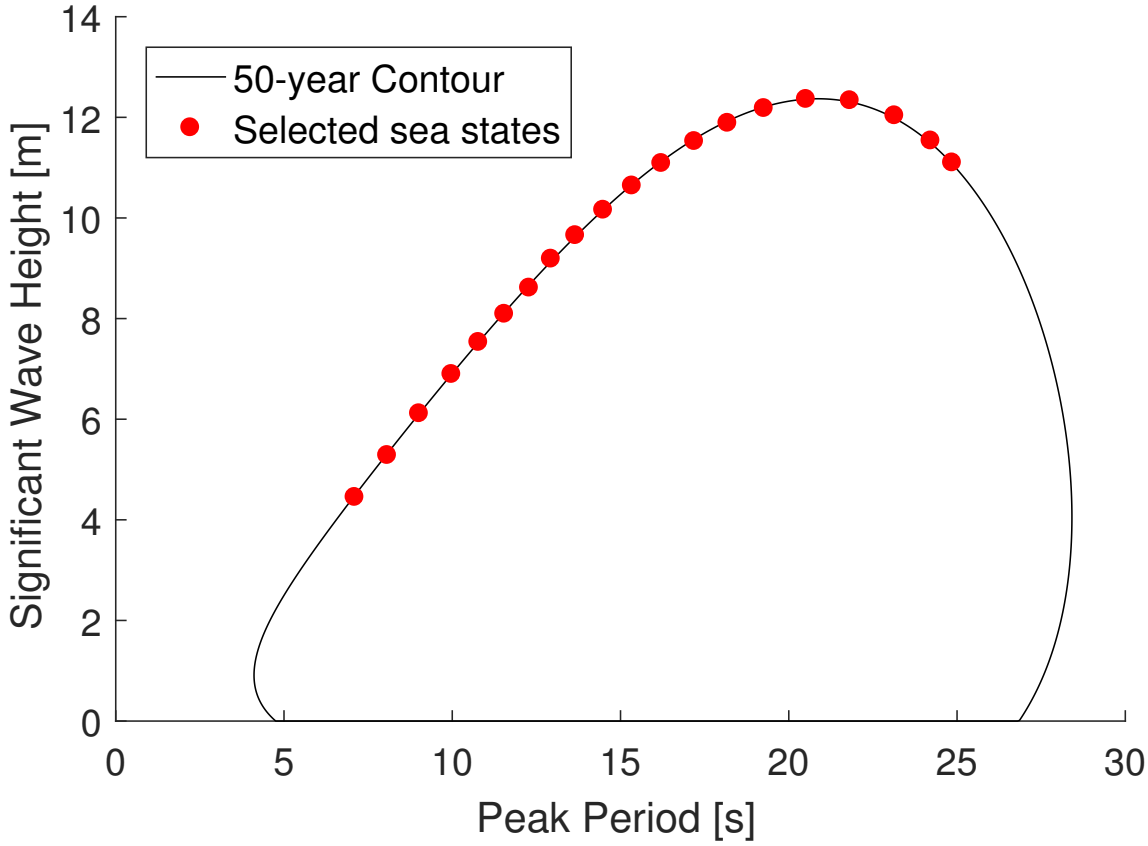

Figure 3.4: Selected sea states along the 50-year contour.

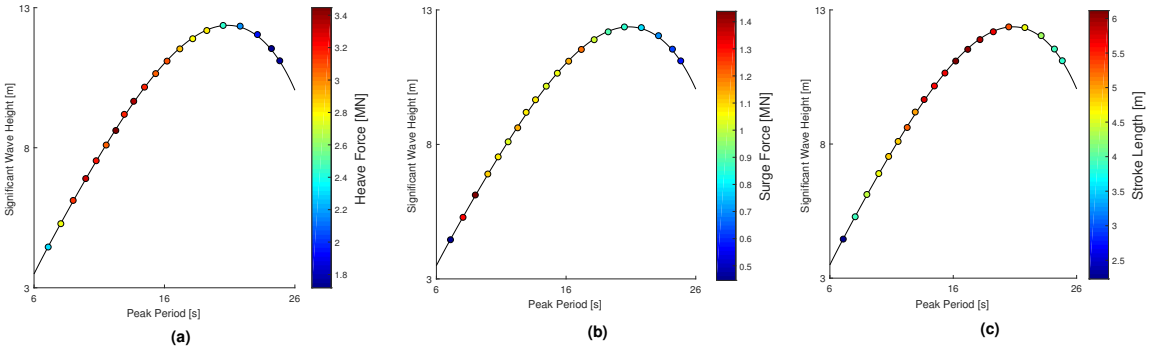

Figure 3.5: Median response values along the 50-year contour for (a) heave force, (b) surge force, and (c) stroke length.

3.3 Results and Discussion

The results from both methods are shown in Table 3.1. In addition to the design loads, the values for the environmental contour method also include the controlling sea state (i.e., the sea state where the highest median load was observed).

Table 3.1: Long-term loads for both methods and for all response variables.

Response	Direct Integration	Environmental Contour Method
Heave Force [MN]	3.49	3.45 (8.6 m, 12.3 s)
Surge Force [MN]	1.60	1.44 (6.1 m, 9.0 s)
Stroke Length [m]	5.82	6.11 (11.1 m, 16.2 s)

For heave and surge force, the answers are as we expect; the direct integration answer is higher than the environmental contour answer. However, that is not the case for stroke length. If a correction factor was applied to the contour method or 3-D IFORM was included in the study, then we would only expect larger answers to emerge. This means that our direct integration method found a 50-year load that is too small. The source for this error can be traced back to the binning scheme that was used for the direct integration method. The binning here is too coarse to provide an accurate representation of the sea state space. Additionally, the weighted average of significant wave height and peak period within each bin should be chosen as the representative sea state instead of selecting a random point. If some sea states exhibit more variability than others, then more simulations may need to be run for each bin. Finer binning is also an option, although the computational time needed would drastically increase.

The 50-year contour also may not be as accurate as is necessary for this analysis. Although the PCA method seems to provide a contour that encapsulates the data well, the limits of the contour, particularly near the breaking wave line, may be overestimating the actual extents of the 50-year metocean extremes. In effect, the errors in our analytical procedures provide two outlets to correct this data; direct integration needs to provide a higher loads and the environmental contour method needs to output lower extremes. In terms of computational time, each method took essentially the same amount of time to run simulations and post process the results. Overall, corrections need to be made in the process of each method to provide more accurate answers.

Chapter 4

Buoy Comparison

4.1 Introduction

Up until now, most of the focus in this report has been on how to quantify a large amount of sea state data into "worst case scenario" data using different statistical approaches and contour methods. This section will look into the accuracy of the original data being analyzed and the effects it can have on a WEC. For all of the previous studies, NDBC buoy data was used. Since the NDBC data is collected using moored buoys, it is a concern that waves larger than the amount of slack in the mooring line would be ignored. Including these large waves when designing a WEC is crucial for energy optimization and efficient structural design. To study how reliable NDBC data is, we will compare it to another method of recording sea conditions using Surface Wave Instrument Float with Tracking (SWIFT) buoys [27]. These buoys are free to drift and have no limitations to the size of the wave they capture. It is to be expected that the NDBC data will show smaller sea states than the SWIFT data. However, the opposite was found.

4.1.1 NDBC

NDBC buoys are deployed all over the world. They are used to measure barometric pressure, wind direction and speed, air and sea temperatures and the wave energy spectra. The geometry of these buoys depends on their location. The hull diameter can range from 2.4 to 12 m. The NDBC uses specific mooring designs for each buoy based on hull type, location, and water depth that can be a combination of chain, nylon, and buoyant polypropylene materials [28]. The NDBC buoy used for this study is a moored, aluminum-hulled, 3m discus buoy. A distinctive feature of discus buoys is that they have spherical hulls. Figure 4.1 shows this type of NDBC buoy [28].

NDBC buoys use accelerometers on board the buoy to measure the heave acceleration with a frequency range of 0.03 to 0.40 Hz [29]. A Fast Fourier Transform (FFT) is applied to transform the data from the temporal domain into the frequency domain. Response amplitude operator (RAO) processing is then performed on the transformed data to account for both hull and electronic noise. It is from this transformation that wave energies and their associated frequencies are derived [30]. From this data we are able to simulate a

corresponding time series and obtain statistical estimates using linear theory. The wave elevation of irregular seas can be written as a sum of wave components recorded.

Figure 4.1: NDBC 3m "discus" buoy (image from `http://www.ndbc.noaa.gov`).

4.2 SWIFT

The Surface Wave Instrument Float with Tracking (SWIFT) buoy was developed to be an autonomous buoy that makes measurements of turbulence at the ocean surface in a wave-following reference frame [27]. Figure 4.2 shows a version 3 (2011) SWIFT along with its specifications. The overall height of this device is 2.15 m (1.25 m draft + 0.9 m mast) with a 0.3 m diameter hull. Onboard instruments make it possible to track the SWIFT in real time while collecting data in 5 minute bursts. These buoys are thrown out into the open water and allowed to drift back to shore (typically during storms). Their missions typically last several hours to a few days. Tests have been conducted to understand how SWIFTs travel with the wind and currents and results show that the SWIFTs drift at about 5% of the wind speed. This response causes some rotation and tilting during wave-following. However, these platform motions have negligible effects on the data [27].

SWIFTs have been refined several times since being developed in 2010 and are still being improved today [31]. The version 3 SWIFT, which includes a Doppler velocimeter to sample the wave spectra with a frequency range of 0.0098 to 0.4902 Hz, is used for part of this study [27]. This version measures the total velocity in separated components. It uses a GPS (Geoforce GT1) to measure the time mean drift velocity and the wave orbital velocities. It is also equipped with a pulse-coherent ADCP (2MHz Nortek Aquadopp HR) mounted on the lower hull, to measure the turbulent fluctuations of velocity. For this study, we are specifically concerned with the vertical motion of the buoy. These SWIFTs include onboard data processing and Iridium telemetry of hourly results. The IMU, or inertial measurement unit, (MicroStrain 3DM-GX335) integrates GPS positions and velocities to provide a complete Attitude Heading Reference System (AHRS) at 25 Hz [31]. The version 4 (2016) SWIFT is also used in this study. The version 4 is very similar to the version 3, though the version 4 is shorter, wider, and uses an upgraded IMU. It has a height of 0.54 m and a hull diameter of 0.45 m. It uses an SBG Ellipse (IMU) to record the AHRS. The AHRS from both versions of the SWIFTs are able to deliver the buoys roll, pitch, heave, surge and sway. The developers of the SWIFTs use MATLAB to then integrate the AHRS data in order to estimate the raw displacements of the buoy. The final SWIFT data, which is used in this study, is the raw vertical displacements which are sampled at 25 Hz.

The vertical displacements are sampled every 12 minutes for a sample duration of approximately 5 minutes. Therefore, for every 1 hour there are 5 sets of data spaced approximately 7 minutes apart. This event is illustrated in Figure 4.3 which shows the vertical displacements (wave elevation) for an hour of SWIFT 19 deployed on April 7th, 2017 off the coast of Oregon.

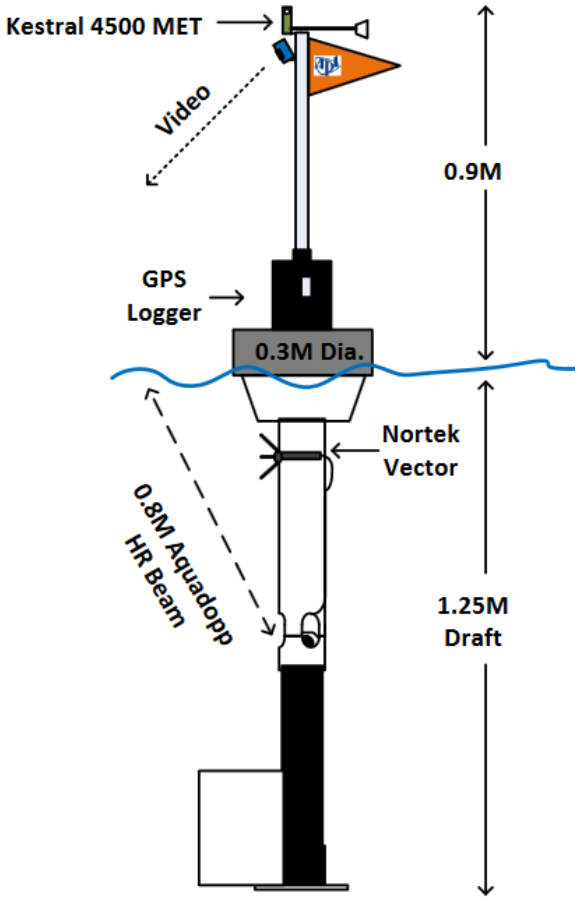

Figure 4.2: Surface Wave Instrument Float with Tracking (SWIFT) version 3 and specifications (image from `http://www.ndbc.noaa.gov`).

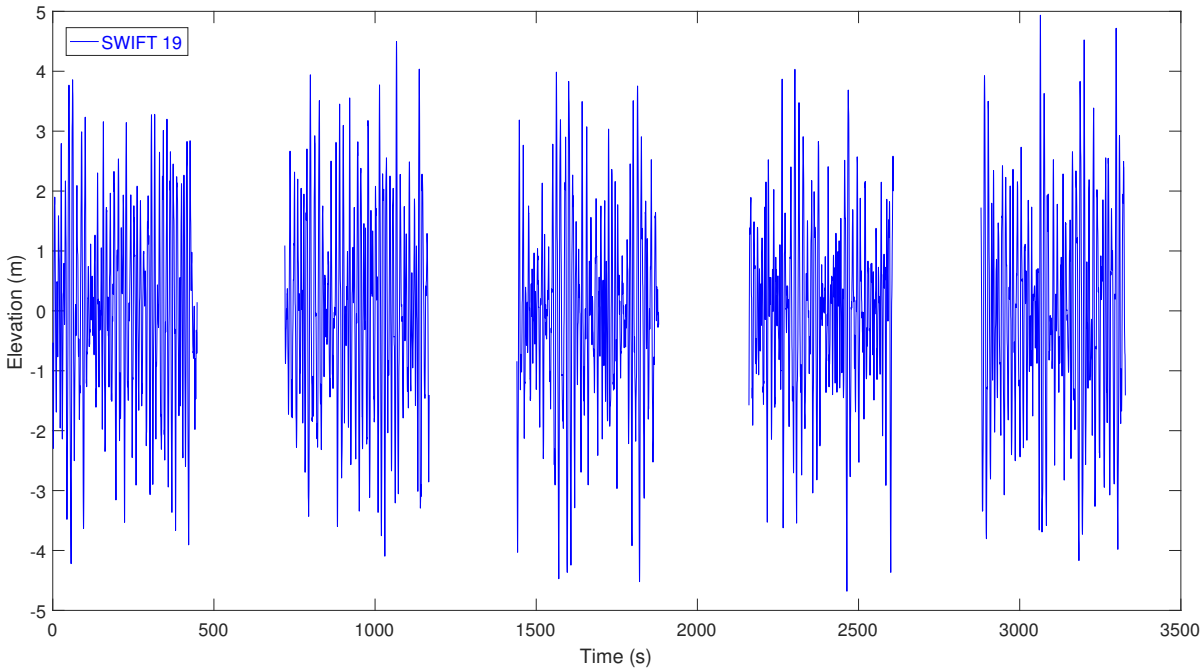

Figure 4.3: Wave elevation data for SWIFT 19 - April 7-9, 2017 hour 15.

4.3 Deployments

For this study, two sets of buoy data are being analyzed and compared. For each set, a pair of SWIFTs were dropped out of a helicopter off the coast of Oregon. These SWIFTs were left to drift freely, collecting data along the way, until eventually washing ashore. The deployments took place on December 11th, 2015, lasting 9 hours and April 7th, 2017, lasting 38 hours. Two version 3 SWIFT buoys were used in 2015 and two version 4 buoys were used in 2017. For each of these deployments, the SWIFTs are compared to NDBC 46050 (Stonewall Bank) which is approximately 25 km away from the deployment site. The locations and drift courses for the deployments are shown in Figure 4.4 and Figure 4.5. The drift paths of the SWIFTs are nearly identical.

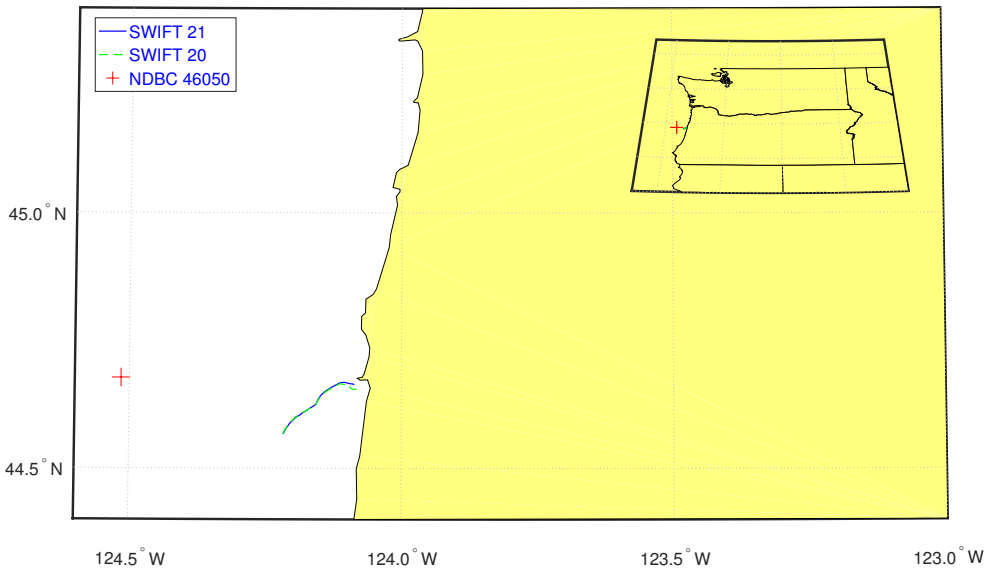

Figure 4.4: Locations and drift paths NDBC 46050, SWIFT 20 and SWIFT 21 on December 11, 2015.

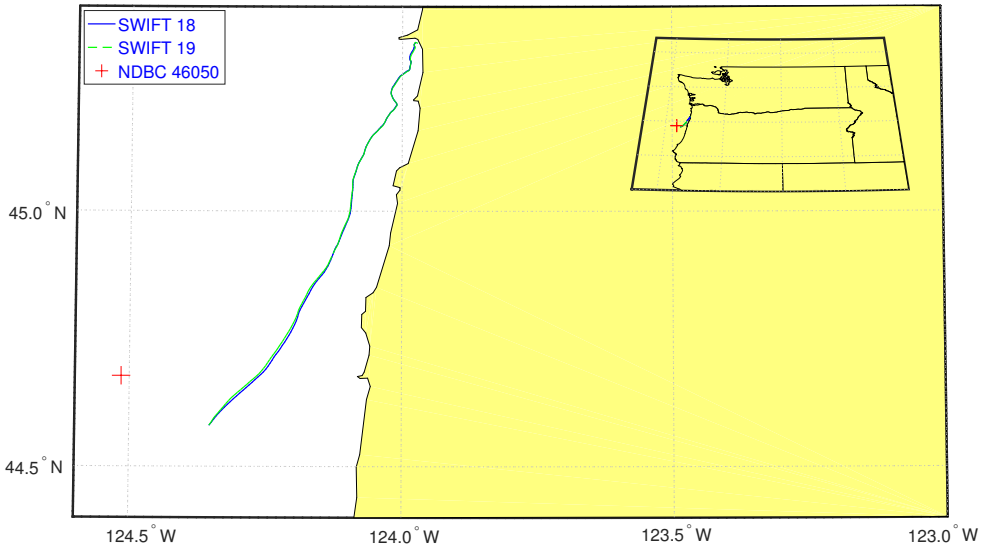

Figure 4.5: Locations and drift paths for NDBC 46050, SWIFT 18 and SWIFT 19 on April 7-9, 2017.

4.4 Results

4.4.1 Comparison - Wave Data

The significant wave heights and wave periods for these deployments are shown in Figure 4.6, 4.7, 4.8, 4.9. These were found using the 15th International Towing Tank Conference (ITTC) recommended calculations of the International Ship and Offshore Structures Congress (ISSC) spectral formulations for open sea conditions, making them dependent upon the wave spectrums recorded by both buoys [32]. As previously discussed in Section 4.2, there are 5 SWIFT points for every 1 NDBC point due to the difference in window length. The significant wave heights recorded by NDBC 46050 are consistently larger than that of the SWIFTs for each deployment. The energy periods recorded have more similitude, but still the energy periods recorded by the NDBC buoys tend to be slightly larger.

The wave height normalized histograms and wave spectra for hour 7 of the 2017 deployment and corresponding NDBC data are shown in Figures 4.10 and 4.11. These reiterate what is shown in Figures 4.6, 4.7, 4.9 and 4.8 by illustrating, that the NDBC is measuring larger significant wave heights.

4.4.2 Comparison - Significant Wave Height

The classical linear theory assumes the surface elevation to be the sum of independent harmonic waves and is therefore a Gaussian distribution. This theory results in a Rayleigh distribution for the prediction of wave heights see, e.g. [33]. Each Rayleigh distribution is associated with a specific significant wave height. That is part of the reason it is such an important parameter to analyze before designing a WEC. The SWIFTs significant wave height and energy period are calculated using only approximately 5 minutes of data. A 5-minute window may not contain enough waves to obtain accurate statistical parameters. For example, the peak elevation of each wave for a single set of SWIFT and NDBC data with a significant wave height of 5.66 m along with the corresponding Rayleigh distribution are described using normalized histograms in Figure 4.12. It should be noted that each buoy encounters a significant wave height of 5.66 m at different times. The SWIFT only encounters 57 individual waves for the probability distribution shown. Whereas, the NDBC data is using a window that is 12 times the length of the SWIFT window. It is shown that the NDBC histogram could be more easily fit to the Rayleigh distribution than the SWIFT. The most collected wave elevation for these two sets of data differs by 1 m. If the SWIFT collected data for a longer amount of time, therefore increasing the sample size, the significant wave height could change, resulting in a better fit to the ideal Rayleigh distribution. Figure 4.13 shows the similarity of the wave spectra associated with these buoys for the significant wave height of 5.66 m.

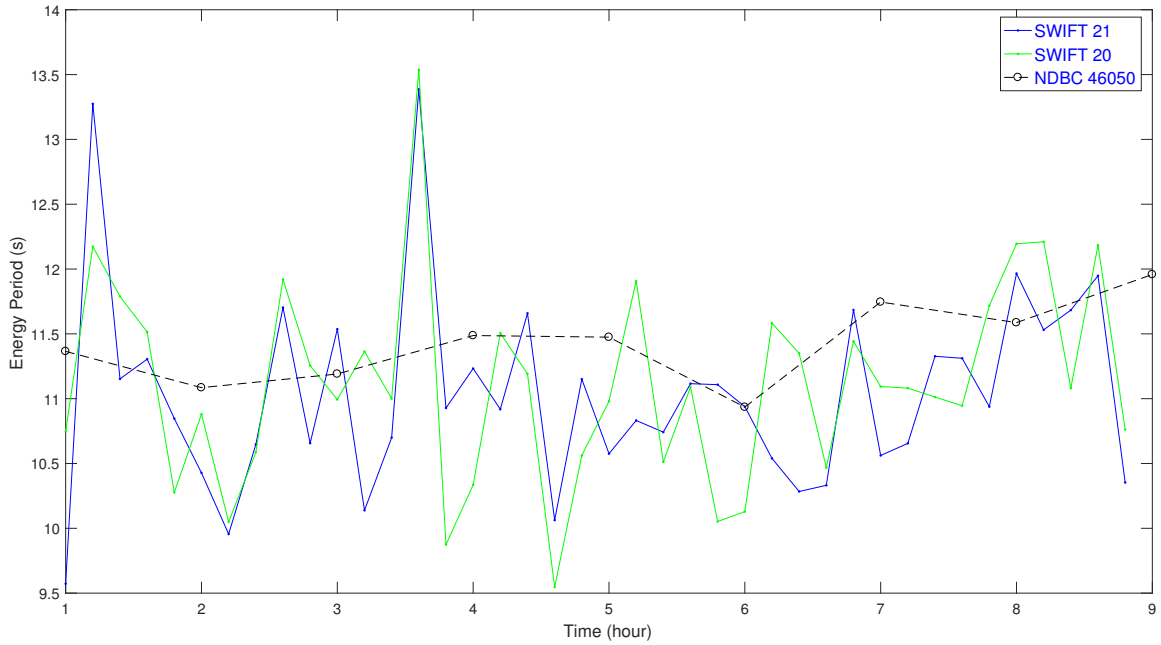

Figure 4.6: Energy periods for December 11, 2015.

4.4.3 Comparison - WEC Results

After comparing the differences in the buoy data, the next step in the analysis was to see how these differences affect the WEC response. The wave elevation time series for each buoy was input into WEC-Sim and the heave PTO forces of a two body point absorber WEC (RM3) were compared [34]. The damping coefficient was set to a range of values to ensure it was not more optimized to one set of data or another. However, it was found that for each damping coefficient chosen, the trend of the differences between buoys remained the same. It should also be noted that the spring stiffness value of the power take off device was set to 0. The local maxima between zero-up-crossings in the PTO force were tabulated and from this the 90th percentile value was found. Figure 4.14 and 4.15 shows the 90th percentile values at their corresponding time for each buoy while the damping coefficient was set to 200,000 N/(m/s). As discussed in Section 2, PTO force is directly correlated to significant wave height. The RM3 simulation results were that of the expected. This confirms that the operational differences and waves captured by each buoy are important to accurately minimize PTO forces.

4.4.4 Comparison - Linear Theory

After finding that the differences between the SWIFTs and the NDBC buoys were constant no matter how they were analyzed, the SWIFTs raw displacement data was compared to its own spectra-formed time series. The transformation from spectra to wave elevation time series was kept identical to the process used when transforming the NDBC data. Figure 4.16,

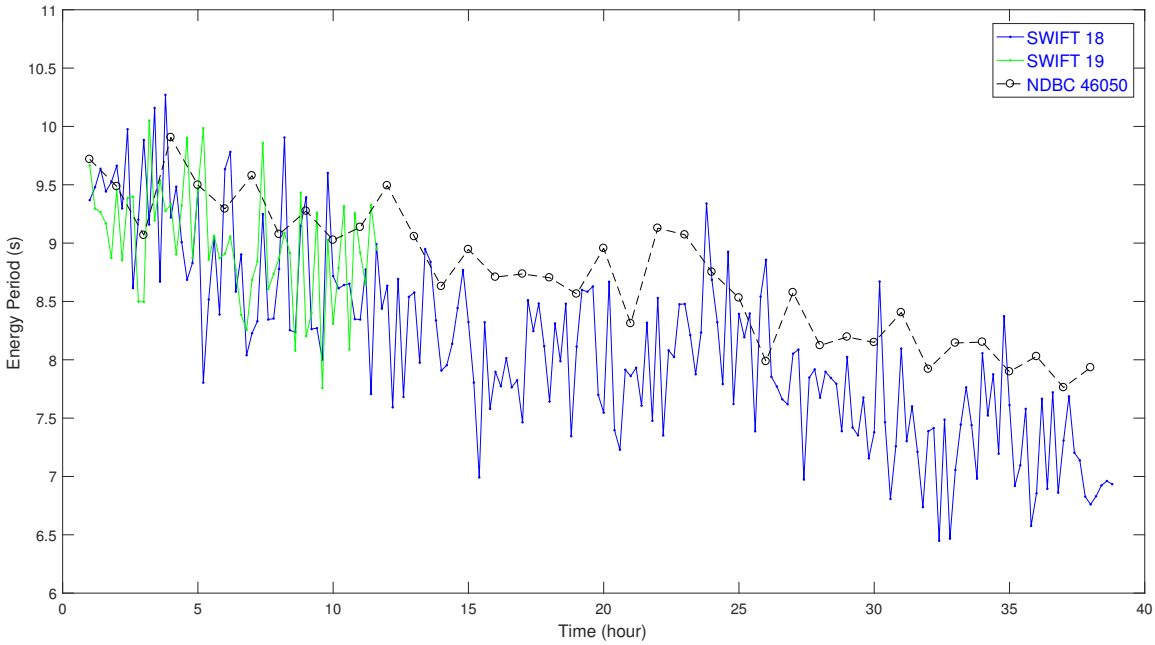

Figure 4.7: Energy periods for April 7-9, 2017.

4.17 and 4.18 show the SWIFT 18's comparison of the raw displacements to the predicted data. Linear theory is an accurate way to estimate the wave elevation time series based on how compatible this data is.

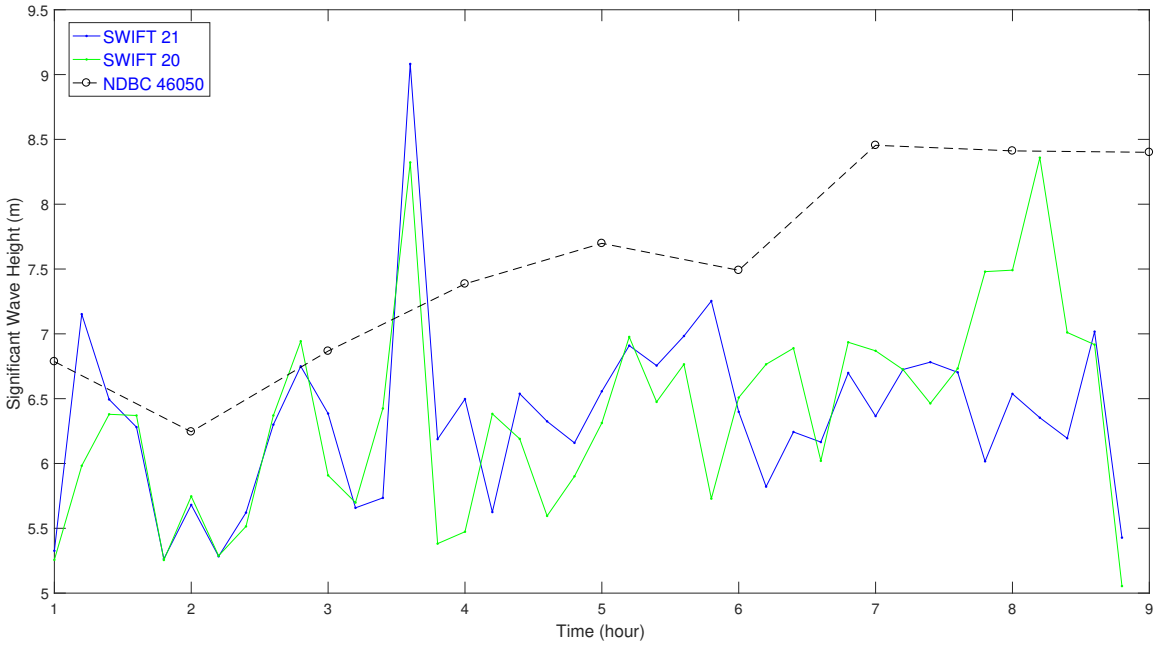

Figure 4.8: Significant wave heights for December 11, 2015.

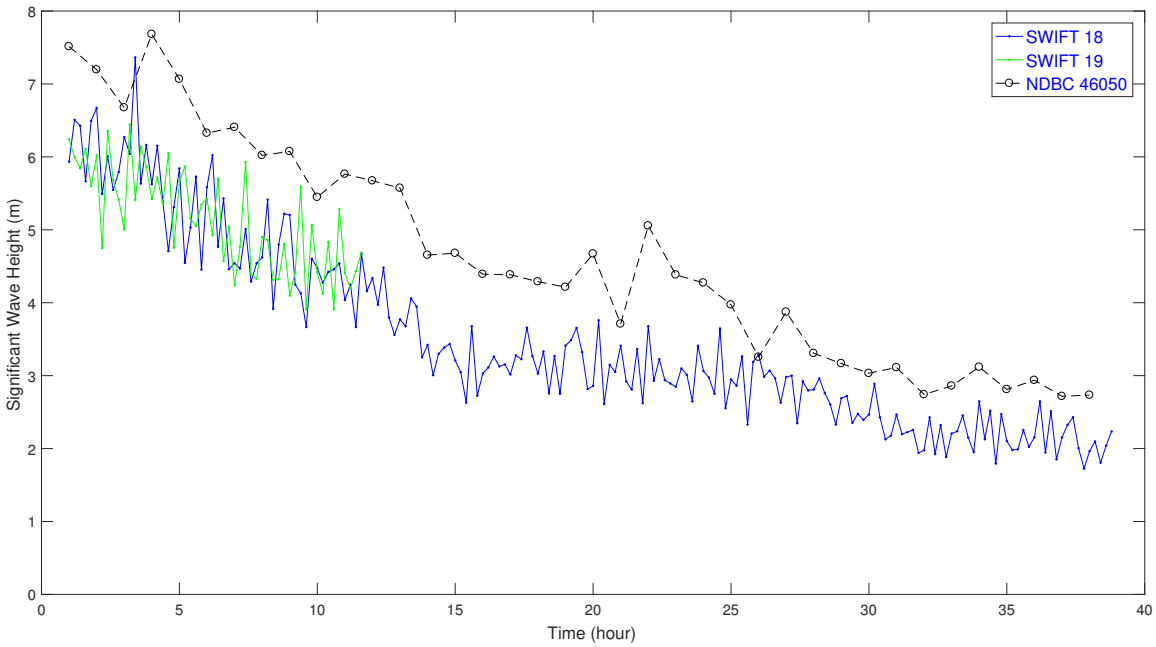

Figure 4.9: Significant wave heights for April 7-9, 2017.

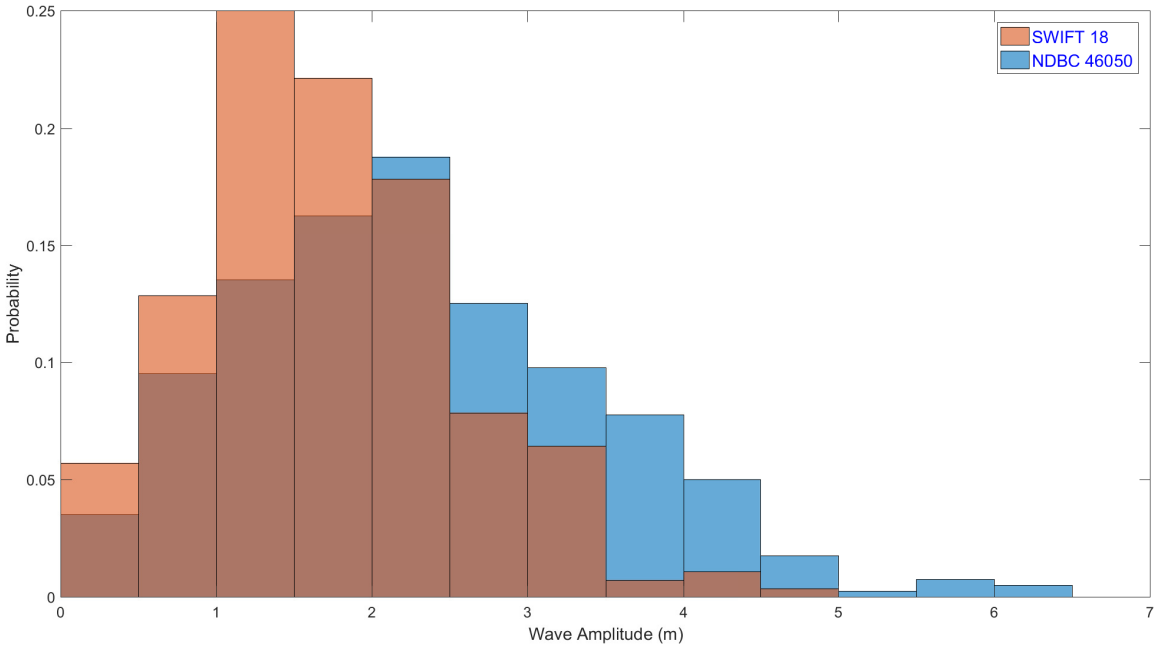

Figure 4.10: Wave amplitude distribution for hour 7 SWIFT 18 and NDBC 24060, April 7-9, 2017.

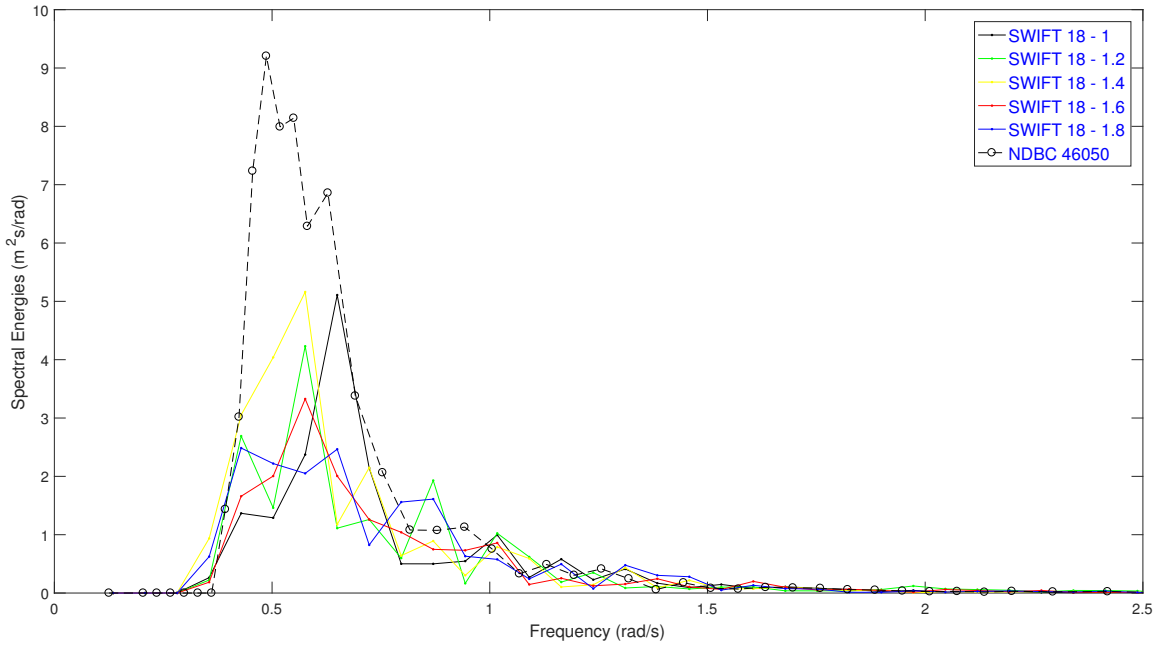

Figure 4.11: Wave spectra for hour 7 SWIFT 18 and NDBC 24060, April 7-9, 2017.

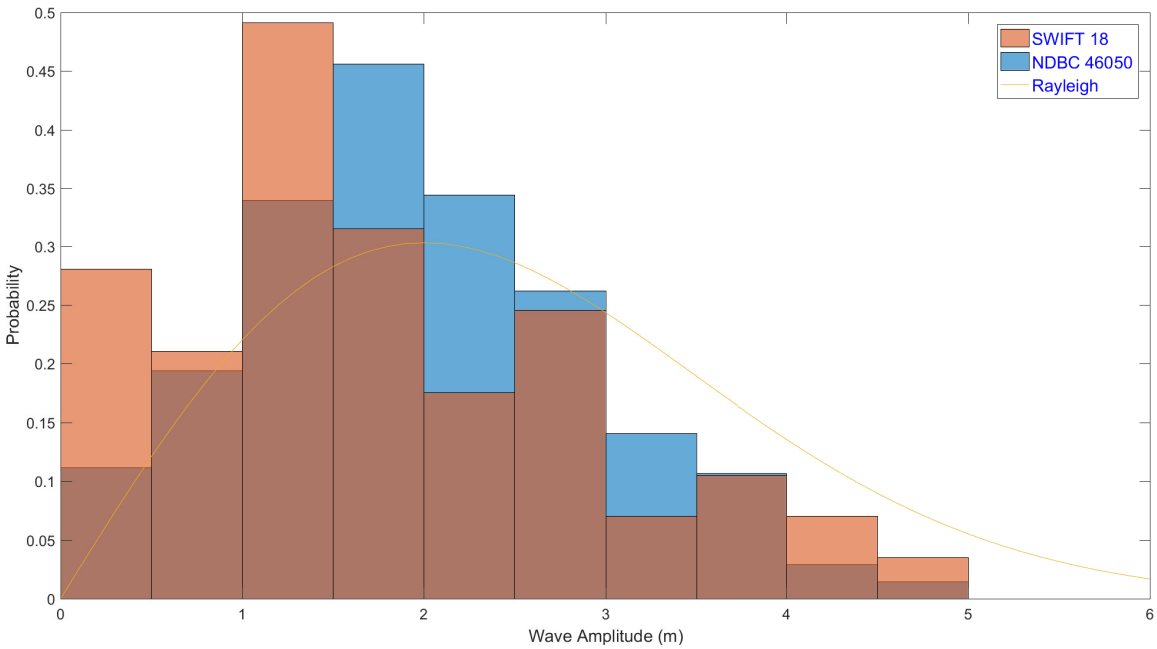

Figure 4.12: Wave amplitudes distribution for significant wave height of 5.66 m SWIFT hour 0.8, NDBC hour 12.

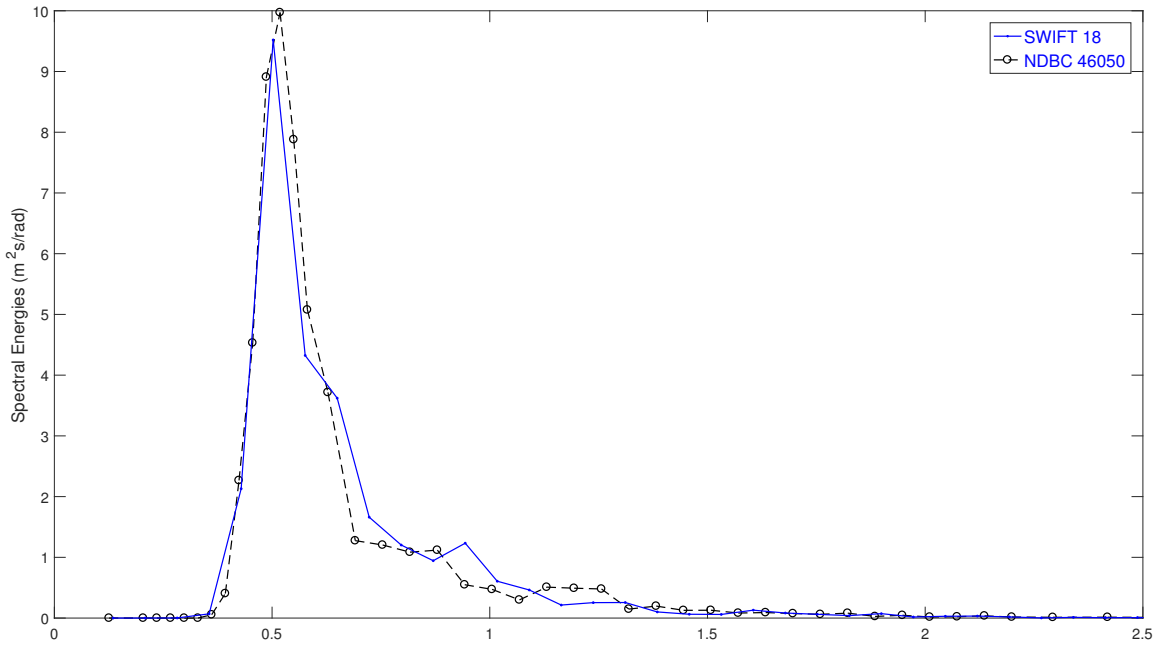

Figure 4.13: Wave spectra for significant wave height of 5.66 m SWIFT hour 0.8, NDBC hour 12.

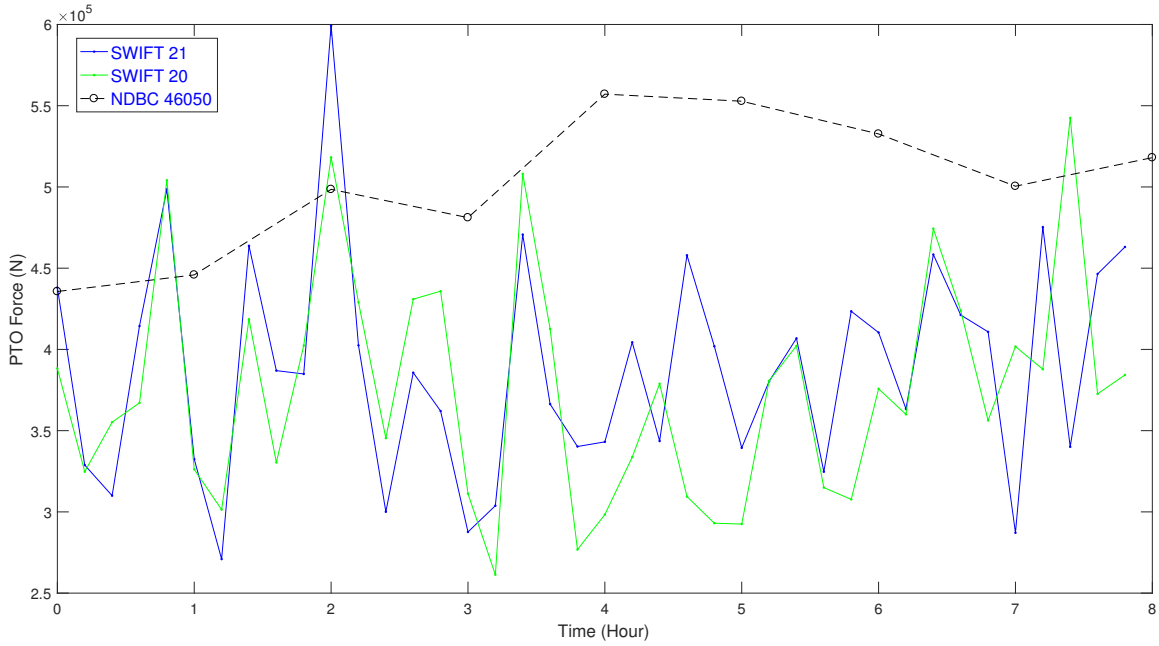

Figure 4.14: 90th percentile value for PTO force for December 11, 2015.

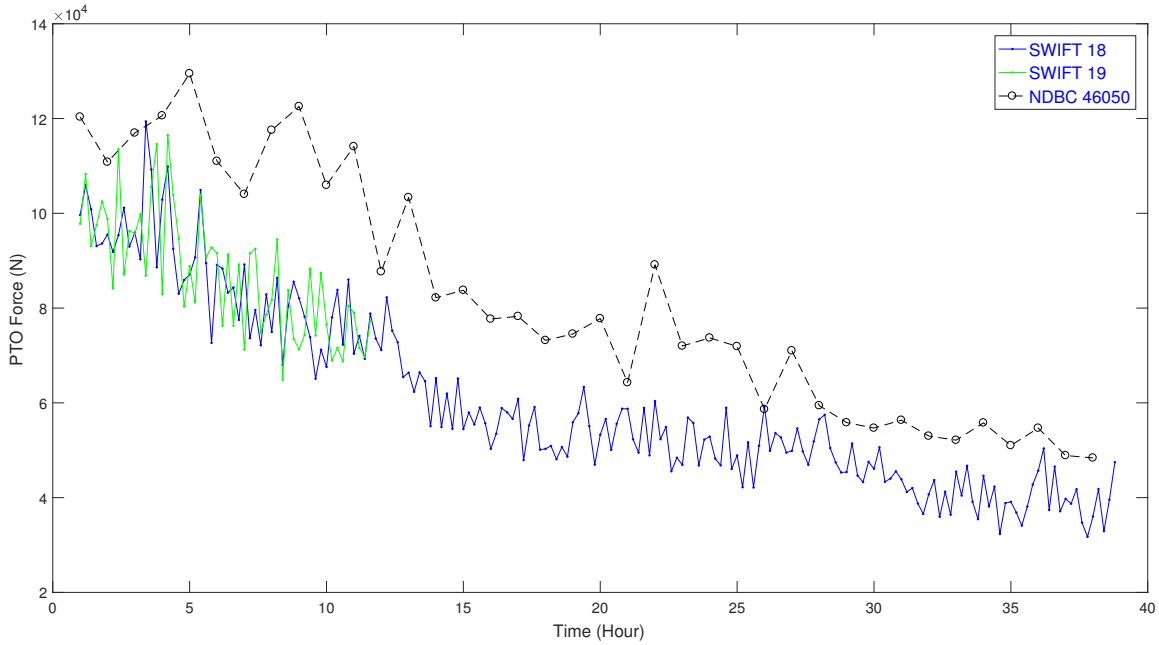

Figure 4.15: 90th percentile value for PTO force for April 7-9, 2017.

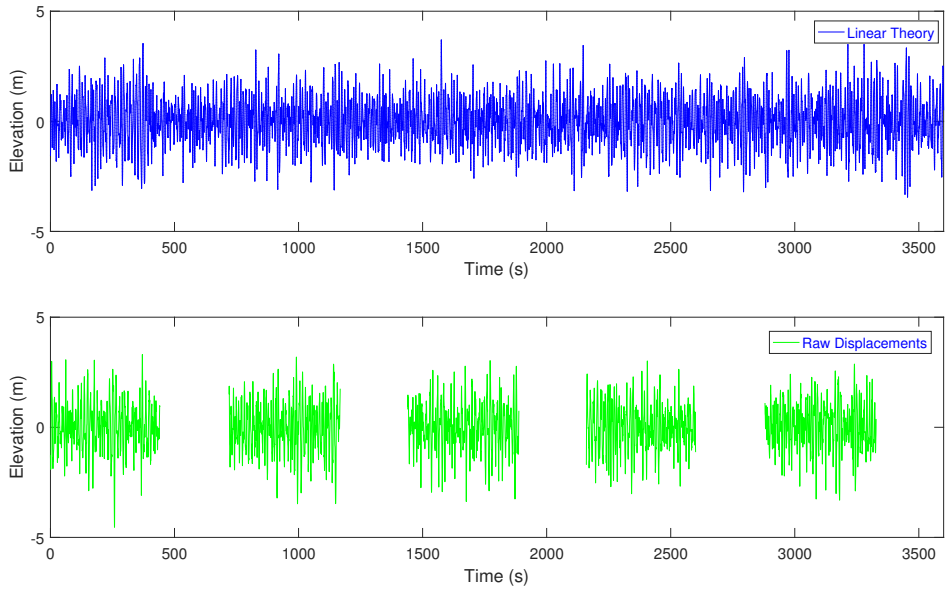

Figure 4.16: Wave amplitude time series for SWIFT 18 April 7-9, 2017.

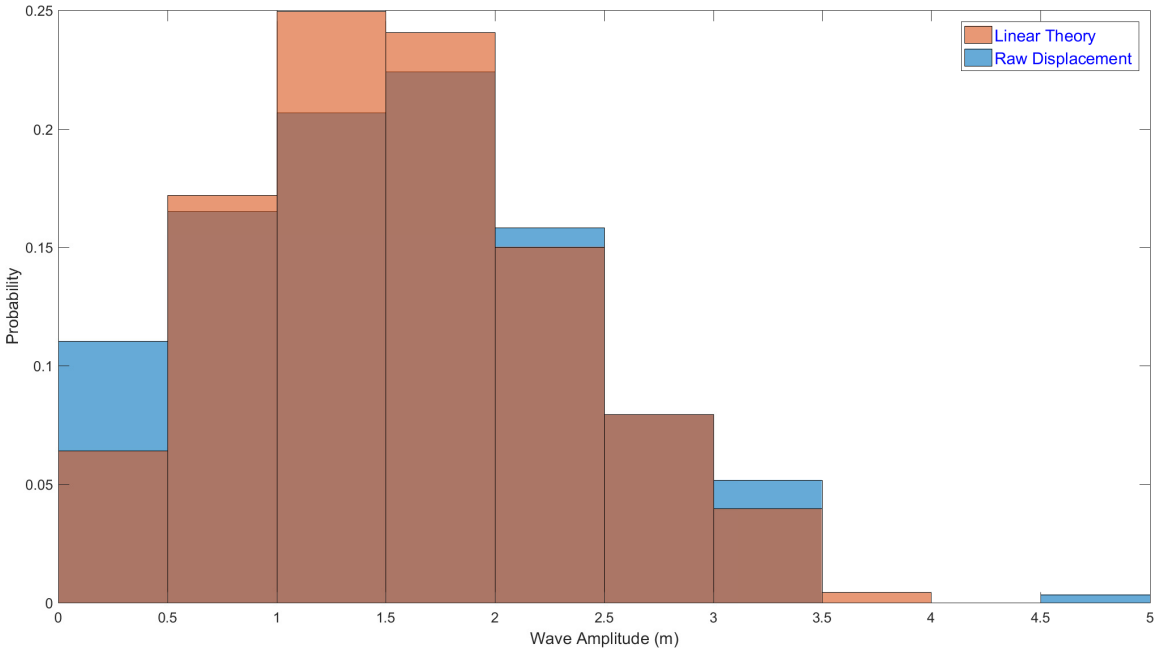

Figure 4.17: Wave amplitude distribution for hour 10 for SWIFT 18 April 7-9, 2017.

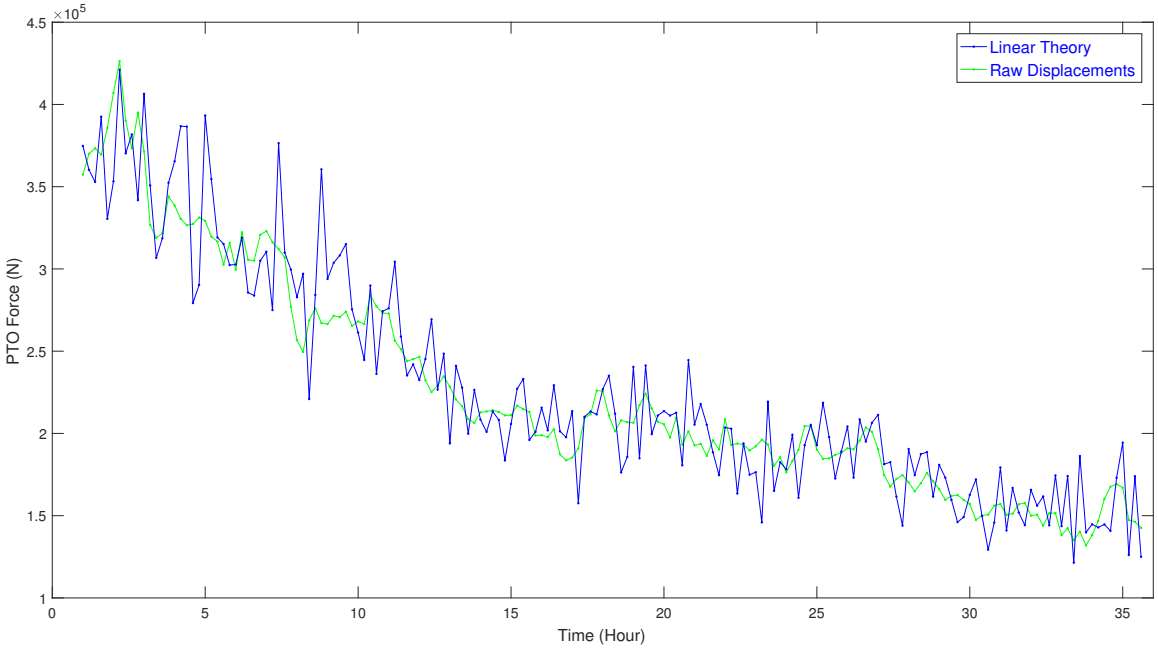

Figure 4.18: 90th percentile value for PTO force for SWIFT 18 April 7-9, 2017.

4.5 Conclusions and Future Work

There are several things that should be noted about the comparison of these different style buoys. First, the distance in the buoys being compared is not ideal. It would be useful to test data that was collected closer together. However, there have not been any deployments that have data for both types of buoys studied in this section. It is known that waves are generally larger offshore; this could be the sole reason for the difference in significant wave heights between the buoys and the resulting WEC response. However, there are still other differences that could affect the results such as size, degrees of freedom, instruments on board, and length of data collections.

Most NDBC buoys have been collecting data for decades. NDBC 46050 has been deployed since 1991. However, NDBC buoys are serviced regularly and all outages are recorded. During the times analyzed in this study there were no known malfunctions of onboard instruments. The processing methods of NDBC have remained the same since 2008. A benefit to the SWIFTs is that they are checked in between every deployment and constantly upgraded. The difference in instruments onboard that collect data could affect the comparison.

Another physical difference is the larger size of the NDBC buoy. SWIFTs have a theoretical natural period of 1.3 s. They were intentionally designed to have a natural period shorter than most ocean waves [28]. The NDBC has a larger natural period, which could cause it to miss short waves. It was an original concern that the mooring of the NDBC could cause it to miss large waves. Although this is not an apparent problem with the comparison, it could still be true.

In the future, it would be beneficial to test these two types of buoys at a much closer location. This could eliminate the skepticism in the aforementioned differences between the two and validate each of the methods. While the SWIFTs are gathering raw amplitude data, the gaps in the data sets and the time window of collection limits the quality. NDBCs have more reliable data and since most WECs are stationary, this data is more applicable to their future development.

Chapter 5

Clustering Analysis

5.1 Introduction

The contouring method introduced has been designed to estimate extreme sea states for individual sites. However, the WDRT toolbox lacks the ability to compare the generated results among different sites. This poses a problem when attempting to characterize ocean sites based on similarity in order to provide more information for WEC placement. To fix this problem, a process of comparison must be introduced alongside the contour methods. Because the process of characterization involves grouping together similar sites, the chosen comparison process is statistical clustering. Statistical clustering is the task of grouping together similar objects. These groups contain objects that are more similar to other objects in the group than they are to objects outside of their group. To determine how similar two objects are, distances are calculated between different metrics from the sites, such as the maximum significant wave height calculated by an environmental contour. How these distances are calculated is dependent on the statistical clustering algorithm in question.

In order to analyze large sets of buoys, however, the data needed to be parsed from the NDBC website. Currently, it is available in large text files for each year the buoy was in service. However, parsing the text files manually would take a very long time. Furthermore, while the WDRT toolbox does contain a script to read in data from the NDBC website, it only does so for one buoy at a time. Thus, a script was created to automate data collection and allow user input as to how much data they want to collect.

5.2 Automated Data-Collection

The Environmental Sea State Contour (ESSC) module from the WDRT was used in order to aid this process. This module can create environmental contours using data from buoys deployed at various sites by the NDBC, and contains implementations of five different contour methods, those being principal component analysis (PCA), Gumbel-Copula, Clayton-Copula, Gaussian-Copula, and Rosenblatt. A separate script was written to automate the use of this module in order to collect the data and statistics necessary to categorize

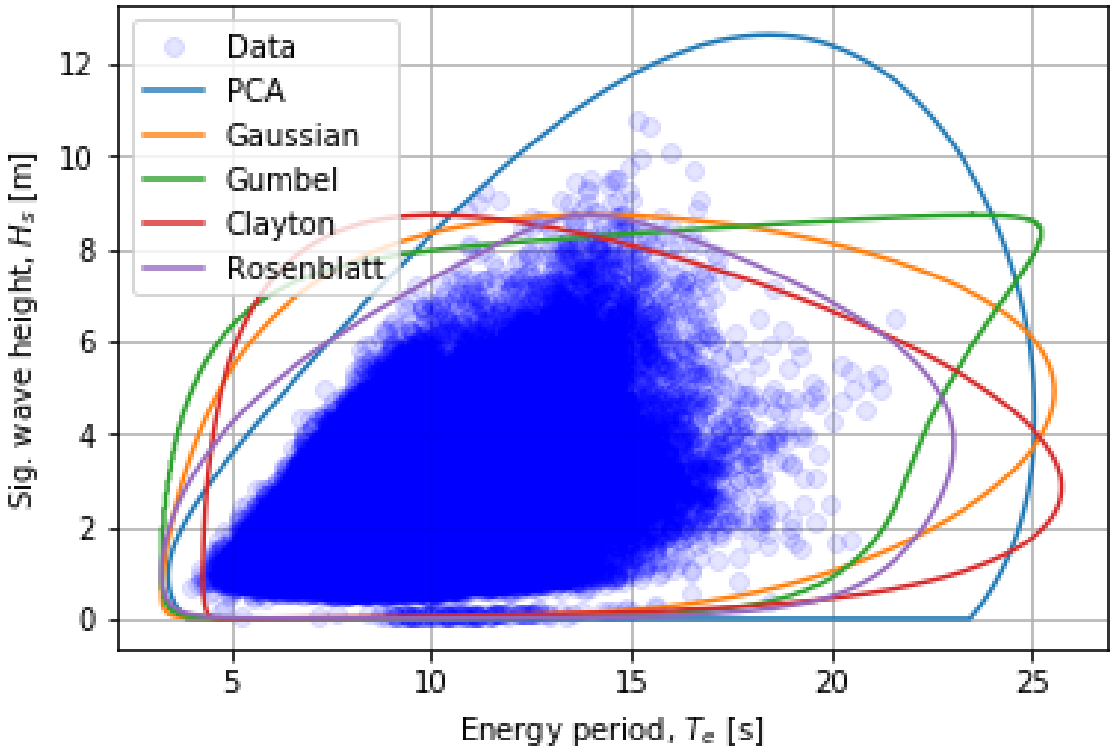

Figure 5.1: An example of the environmental contours generated by the ESSC module of the WEC Design Response toolbox.

larger oceanic regions. Figure 5.1 shows a range of environmental contours generated for NDBC 46022.

In order to use these discrete sites to analyze larger regions, the aforementioned script scans the NDBC website (`www.ndbc.noaa.gov`) for buoys with 15 years worth of data or more. The latitude and longitude for these buoys is also automatically gathered, and is used to sort each site into one of five different regions: the East Coast, West Coast, Gulf of Mexico, Great Lakes, and Hawaii. Figure 5.2 shows a map of the sites considered in this study.

Once the sites are sorted by location, each of the previously mentioned contour methods are run on each site, and up to as many sites at once as the user has CPU cores via multi-processing in order to speed up this lengthy process. While multi-threading is generally the preferred form of parallelization, Python only offers functionality for multi-processing due to a restraint put into the language that only allows one thread to be running at any time (known as the "Global Interpreter Lock" or "GIL"). When the contour methods are done running, the maximum significant wave height (H_s) and energy period corresponding to that maximum wave height (T_e), or in other words, the x value (T_e) and y value (H_s) of the global maximum of each contour plot is obtained. These max values are then stored into separate .csv files depending on the oceanic region they were previously sorted into. Other statistics

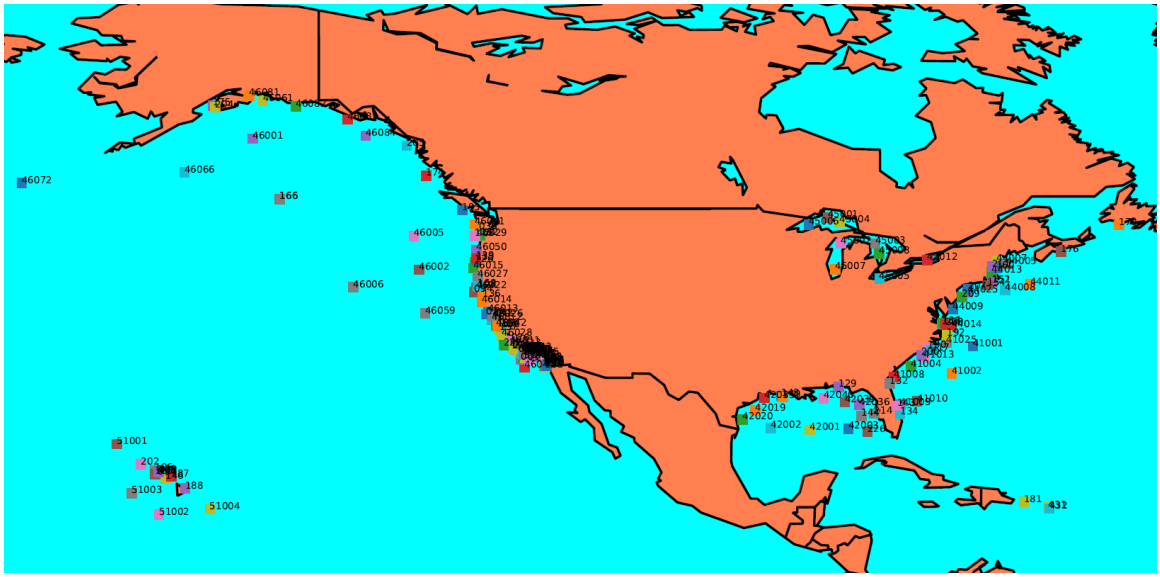

Figure 5.2: Map of all the sites used for this study.

are recorded from this data as well, such as the maximum and minimum H_s and T_e out of all the contour methods, the difference between the two in numerical and percentage form. Storing the data in a light-weight format like this gives an easy way for one to extract the data, or use any .csv readers mathematical functionality, for use in any sort of analysis.

Automating the data collection process has made it easier to obtain relevant NDBC buoy data to use in further analysis. Clustering, as described in the introduction, is the method of analysis used. We decided to compare the k-means and mean shift algorithm to determine which to use, due to the level of documentation available for those methods.

5.3 k-means Algorithm

k-means is a clustering algorithm that groups parameters together based upon a distance measure between each individual parameter. The algorithm tries to minimize the distance measure between each individual parameter within a cluster, while finding k number of clusters. The k-means algorithm takes an integer k and a set of n data points within a total set $\mathcal{X}$, and attempts find k number of centers $\mathcal{C}$ to minimize the function

$$\phi = \sum_{x \in \mathcal{X}} \min_{c \in \mathcal{C}} \|x - c\| \tag{5.1}$$

From the found centers C, nearby data points that satisfy the above equation are grouped according to which cluster center they are closest to. Traditionally, k-means is calculated with the following iterative process: [35]

1. Arbitrarily pick k cluster centers $\mathcal{C} = \{c_1, c_2, ...c_k\}$

2. For $i \in 1, 2, ...k$ set $\mathcal{C}_i$ to be the set of points in $\mathcal{X}$ that are closer to c_i than $c_j \forall j \neq i$
3. For $i \in 1, 2, ...k$ set $c_i = \frac{1}{|\mathcal{C}_i|} \sum_{x \in \mathcal{C}_i} x$
4. Loop steps 2 and 3 until $\mathcal{C}$ converges

However, this method is not the most optimal way to compute k-means. This is due to the dependence on arbitrarily chosen cluster centers. In common practice, the starting cluster centers are just random points. Because the initial cluster centers are chosen at random, if the algorithm is computed many times different cluster centers will be found. This can drastically change the results, especially if the input is a relatively sparse data set. Because of this issue, we use a modified initiation method for the clusters, called k-means++.

5.3.1 k-means++

K-means++ removes the random choice for initializing cluster centers, and makes the process more methodical. [36] It uses the following steps:

1. Define $D(x)$ to be the shortest distance from a data point x to the closest center already chosen
2. Take a center c_1 chosen uniformly at random from $\mathcal{X}$
3. Take a new center c_i, choosing $x \in \mathcal{X}$ with probability $\frac{D(x)^2}{\sum_{x \in \mathcal{X}} D(x)^2}$
4. Run k-means, ignoring the step for arbitrarily choosing cluster enters

5.3.2 Potential drawbacks

There are some drawbacks to using k-means. While the initializing algorithm prevents the randomization of cluster centers, the algorithm still assumes that all optimal clusters are spherical. This means that the calculated clusters may not necessarily match the overall shape of our data, especially with the relatively sparse data set used in this analysis. Rather than cluster directly on the NDBC buoy data, we clustered based on the data gathered from the generated contours. This means that rather than clustering thousands of raw data points, the algorithm clusters only as many data points as there are applicable buoys. Another issue is the number of clusters to find in k-means needs to be specified before calculation. If the user input is too large, it could cause significant issues with finding accurate clusters; too many would result in every data point counting as an outlier, while too few would result in the entire data set being a part of a single cluster. Finally, due to the geometric nature of k-means, outliers in the data can skew the placement of the cluster centers. Despite the fast runtime of k-means, these factors caused us to look at another clustering algorithm, known as Mean Shift.

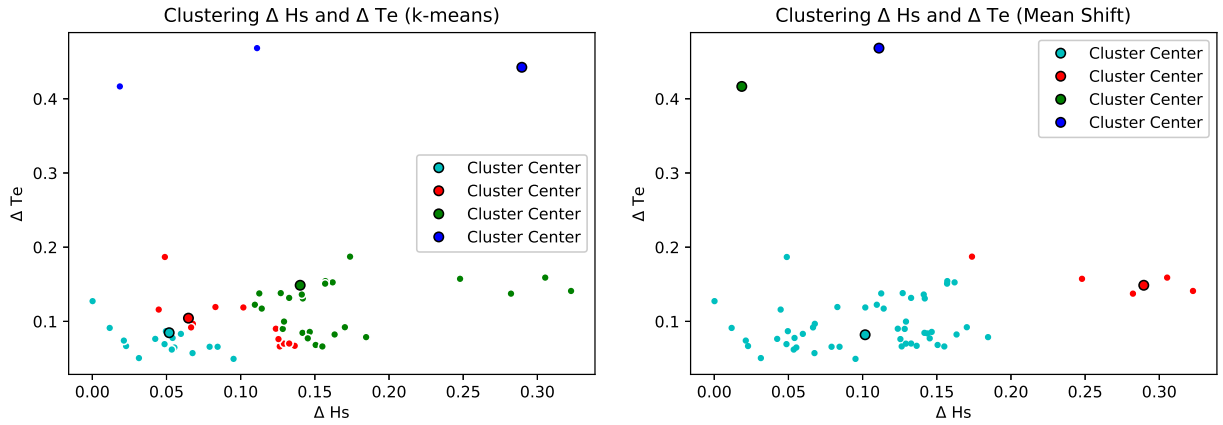

(a) K-means.

(b) Mean shift

Figure 5.3: Clustering west coast buoys.

5.4 Mean Shift Algorithm

Mean Shift is a clustering algorithm that looks for the maxima of a density function, given a sampled set of data $\mathcal{X} = x_1, x_2, ...x_i$. In short, it creates a function to measure the density, or how many data points are close together, and tries to find where that function obtains its maximum value. A kernel $\mathcal{K}(x)$ is defined, where a kernel is a weighting function used to estimate density functions for the sampled set of data $\mathcal{X}$. A set $\mathcal{S}$ is also defined, which contains all the data points x such that $\mathcal{K}(x) \neq 0$. We look for the weighted density in the sampled set of data, defined as

$$m(x) = \frac{\sum_{x_i \in \mathcal{S}(x)} \mathcal{K}(x_i - x)x_i}{\sum_{x_i \in \mathcal{S}(x)} \mathcal{K}(x_i - x)} \tag{5.2}$$

Once $m(x)$ is calculated, we set $x = m(x)$, and repeat this estimation, or shift, until $m(x)$ converges to a point, which is then denoted as a cluster center [37]. What is important to note is that this iterative process shifts the data set $\mathcal{X}$ over as well, in order to ensure the points are all similar within the calculated cluster centers [38]. Figure 5.3 shows a visual comparison of the k-means and Mean Shift algorithms. In the k-means algorithm, we see that the blue cluster, denoting outliers, is far away from the outliers in the top left. In addition, the values in the bottom right look more densely packed than the values in the bottom left, which would imply that the entire bottom right would be an entire cluster of its own. However, it is split into 3 clusters. Compare this with the mean shift clustering, where we see that the bottom right is an entire cluster of its own, and the values in the bottom left are also in their own cluster.

The choice of which algorithm to use took into consideration the shape of the data. Our data set is sparse, and prone to outliers. In addition, our data set is nonspherical. Because

of these qualities, k-means would generate poor clusters and cluster centers. However, Mean Shift would not be as affected by these qualities, as the algorithm is designed to be used with nonspherical clustering. To confirm our choice of using Mean Shift, we calculated the Silhouette Coefficient of the two methods on the same data set.

5.5 Silhouette Coefficient

The Silhouette Coefficient is a validation method for ensuring clustered data is consistent. It measures how similar data is to its own cluster compared to data in other clusters. To calculate the Silhouette Coefficient $s(i)$, we first define $a(i)$ to be the average dissimilarity to all other objects with a chosen cluster $\mathcal{A}$. It is a distance measure from each data point within $\mathcal{A}$ to the chosen data point i. We now compute a distance measure from the data point i to the data points in a cluster $\mathcal{C}$, which is the average dissimilarity of i to all objects within $\mathcal{C}$, called $d(i, C)$. [39]

We now define another parameter, $b(i) = \min d(i, C)$. This parameter defines the cluster that is the nearest neighbor to the data point i. We can now compute the Silhouette coefficient s(i) to be:

$$s(i) = \begin{cases} 1 - \frac{a(i)}{b(i)}, & \text{if } a(i) < b(i) \\ 0, & \text{if } a(i) = b(i) \\ \frac{b(i)}{a(i)} - 1, & \text{if } a(i) > b(i) \end{cases}$$

This equation can also be expressed as:

$$s(i) = \frac{b(i) - a(i)}{max[a(i), b(i)]}$$

From the equations above, we can see that $-1 \leq s(i) \leq 1$ for each data point i. A larger positive value indicates a higher level of consistency among the data inside each cluster, while a negative value indicates a poor level of consistency within the cluster [39]. The Silhouette Coefficient was used to determine whether the mean shift algorithm or the k-means algorithm should be implemented. Table 5.1 shows the silhouette coefficients for the cluster regions. In all data sets used, the Silhouette Coefficient for Mean Shift was larger than the Silhouette Coefficient for k-means for the same number of clusters. Because of the higher Silhouette Coefficient, the Mean Shift algorithm was implemented. This means that the accuracy of the cluster centers calculated by the Mean Shift method is higher than the accuracy of the cluster centers calculated by the k-means method, and therefore the data is more consistent within Mean Shift clusters.

Table 5.1: Silhouette coefficient test results.

Number of Clusters	Geographic Location	k-means++ Coefficient	Mean Shift Coefficient
4	West Coast	0.412	0.598
3	East Coast	0.332	0.581
4	Gulf of Mexico	0.429	0.545
5	Hawaii	0.011	0.426
3	Great Lakes	0.706	0.706
5	All Sites	0.192	0.558

5.6 Clustering Results

For our purposes, we clustered using two normalized inputs: the maximum significant wave height (H_s) calculated by any of the contour methods, and the energy period (T_e) at the calculated H_s value. This will determine the greatest possible maximums detected by the contour methods, and clustering them together will show what regions have similar expected extremes. This data was gathered from 56 NDBC buoys, each containing 15 or more years of measured data. From these 56 buoys:

9 of the buoys are found in the Gulf of Mexico.

4 of the buoys are found off the coasts around Hawaii.

18 of the buoys are found off the West Coast.

9 of the buoys are found within the Great Lakes.

16 of the buoys are found off the East Coast.

Using this data, the clustering algorithm found 3 clusters and 2 outliers. The results of this analysis are shown in Figure 5.4.

Each data point in this graph represents the calculated contour's max H_s and the T_e values. Different colors represent different clusters, so all cyan points belong to the cyan cluster, all red points belong to the red cluster, and so on. There are 5 key takeaway points from this graph obtained by comparing the generated chart to our input data.

1.) Cyan clusters contain all 9 NDBC buoys located in the Gulf of Mexico, 9 buoys located in the Great Lakes, some members located off the East Coast, and some members located off the coast of Hawaii.

2.) Red clusters contain 7 buoys located on the East Coast, 11 buoys located on the West Coast, and 2 buoys located off the coast of Hawaii.

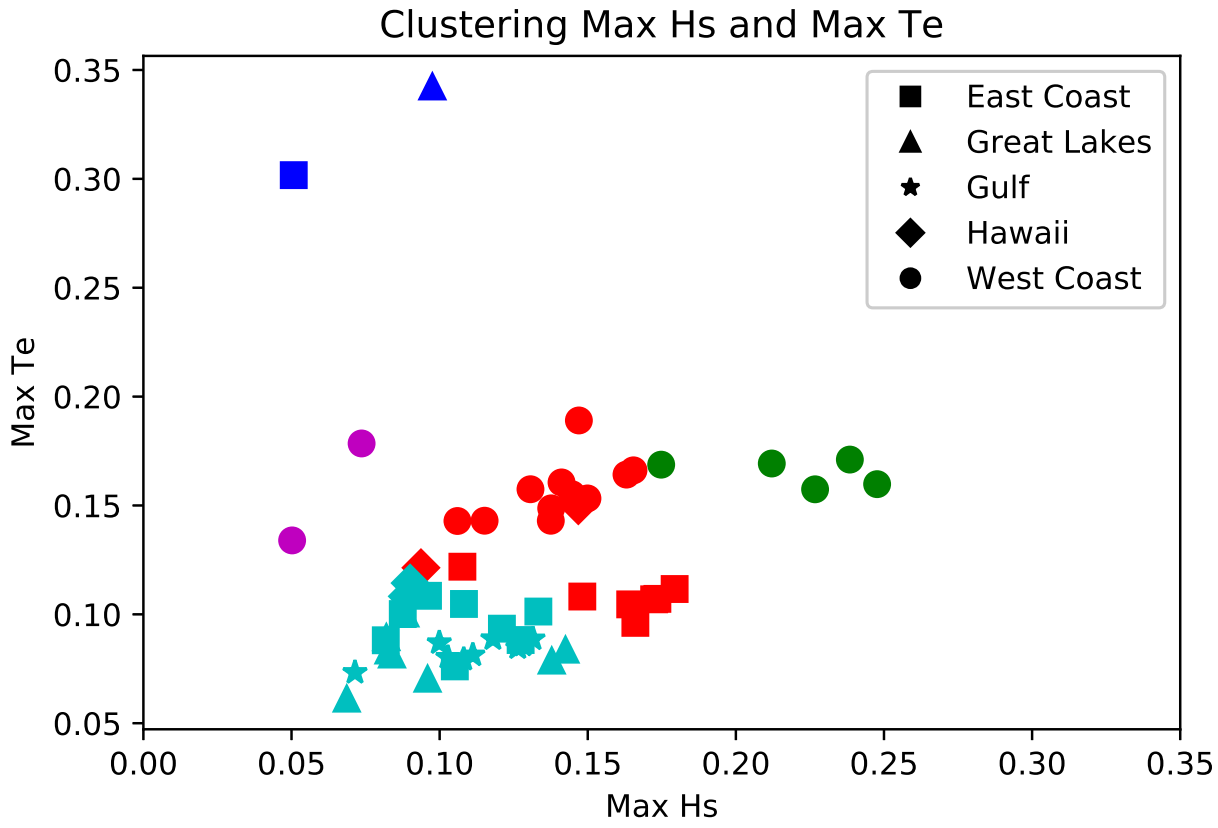

Figure 5.4: Clustering results.

3.) Green clusters contain 5 buoys located on the West Coast.

4.) Magenta clusters contain 2 buoys located on the West Coast.

5.) Blue clusters contain 1 buoy located on the East Coast and 1 buoy located within the Great Lakes.

This appears to imply that for expected extremes, the West Coast is more likely to have extreme waves with a large H_s and T_e when compared to the East Coast and Hawaii. In addition, the Great Lakes has some of the smaller expected extremes, but is also very susceptible to outliers. By quantifying this information, we can determine similar regions of extreme sea states, and from this define characteristics for WEC placement. For example, a WEC that will suffer damage from large waves might be better placed on the East Coast, and a WEC that can withstand rogue waves would be best placed in the Great Lakes.

One important aspect is that there appears to be a natural grouping occurring among all of the different clusters that Mean Shift is not detecting. For example, the buoys on the West Coast all have a narrow band where the max T_e can be found, and the members in the Gulf of Mexico are all contained within very small intervals in H_s and T_e. This is known as a natural grouping, where its clusters are inherently grouped together within the original data set. Because these clusters are more visually apparent, due to their shape, they can be missed with most unsupervised clustering algorithms, such as Mean Shift. However, it is possible to implement another type of clustering algorithm, called supervised clustering, to group together data points based on their natural groupings.

5.7 Future Work

Future work will involve refining the existing Mean Shift algorithm and its implementation into the WDRT Toolbox. Currently, it scores at an average Silhouette Coefficient of 0.65. While this is good, there are methods that can be implemented to increase the score, such as using a more accurate method to calculate the bandwidth. Another avenue for future work is figuring out what variables are the best to cluster in order to find information in extreme condition trends. While the maximum values from the contours might provide valuable insight into extreme condition trends, they may not be the most optimal variables to cluster overall. In addition, due to the need for visualization, only 2-dimensional cluster analysis has been performed. Future analysis may involve more variables, such as taking the maximum values from each calculated contour and clustering them all together. Finally, due to the revelation of natural groupings, research into supervised clustering may take place.

Chapter 6

Contour Evaluation

6.1 Introduction

In order to build structurally and economically efficient WECs, it is essential to be able to forecast long-term sea conditions that the WEC will have to endure in a given location. Creating environmental contours based on hindcast buoy data was first proposed in [40] and is still a frequently used method of accomplishing this. Environmental contours take ordered pairs of observed sea state data and determine an area of observations in which exceeding them could potentially elicit extreme structural responses in a given return period (for higher combinations of H_s and T_e). This study uses two commonly used variables - significant wave height (H_s) and energy period (T_e).

Figure 6.1 shows ordered pair observations of H_s and T_e from 1993-2016 for buoy 46022 located off the California coast. The data shows a recognizable pattern of dependence. This makes sense intuitively that a waves height (H_s) will be related to/dependent upon a variable relating to its width (T_e). In order to generate an environmental contour, a joint distribution of the two variables must be estimated. The dependency of the two variables makes modeling a joint distribution far more challenging.

Since the original environmental contour method was first proposed, many additional contour methods have been developed. Where these methods all primarily differ is the way in which they attempt to capture the dependency between the two variables. Some examples, which will be analyzed in detail in this study, are described below.

- The Rosenblatt Contour, outlined in [1], involves the Rosenblatt transformation and the Inverse - First Order Reliability Method (I-FORM).

- The PCA Contour, as developed in [1], uses principle component analysis to transform the two sea state variables into two new uncorrelated variables and then uses those to generate the contour.

- The Gaussian, Clayton, and Gumbel Contours use a copula to capture the dependency between the two variables. Each separate copula structure will generate a different shape of environmental contour.

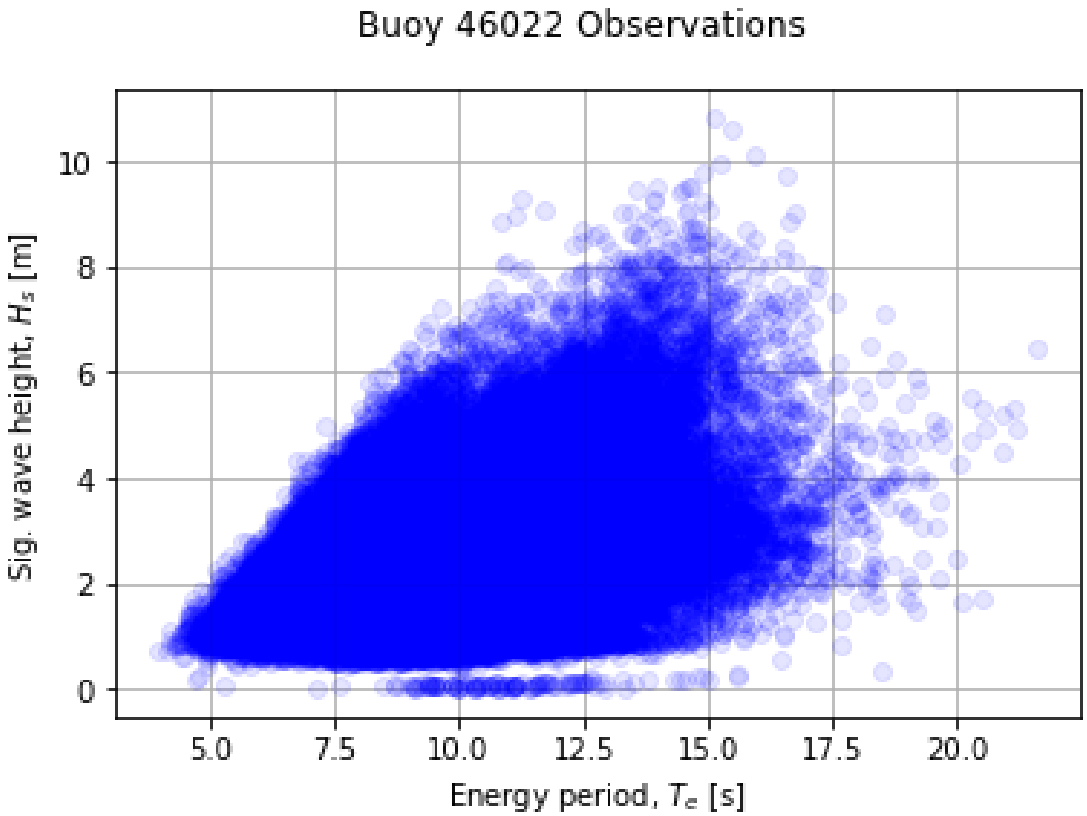

Figure 6.1: 24 years of ordered pair observations of H_s and T_e show a relationship between the two.

All of the above contour methods are available for implementation in the Extreme Sea State Contour (ESSC) module of the Wave Energy Converter Toolbox (WDRT).

6.2 Contour Generation

6.2.1 Model Fitting

In order to create a joint distribution, the marginal distributions must first be established. Four of the five methods (all but the PCA method) considered use maximum likelihood estimation (MLE) to fit a 3-parameter Weibull distribution for the marginal distribution of H_s:

$$f_{H_s}(x) = \frac{\beta}{\eta}\left(\frac{x-\gamma}{\eta}\right)^{\beta-1} e^{-\left(\frac{x-\gamma}{\eta}\right)^{\beta}} \tag{6.1}$$

where β is the shape parameter, η is the scale parameter, and γ is the location parameter. This is a slightly simplified choice of the marginal distribution which can be found in [41]. The five methods primarily differ in how they fit the second marginal distribution.

Rosenblatt Method

Instead of fitting a marginal distribution to T_e, this method fits a conditional distribution to T_e conditioned on H_s. This is achieved by ordering the values of H_s, sorting the corresponding T_e values into bins, and then fitting a separate lognormal distribution to the T_e values in each bin:

$$g_{T_e|H_s}(x) = \frac{1}{x}\frac{1}{\sigma\sqrt{2\pi}} exp\left(-\frac{(\ln x-\mu)^2}{2\sigma^2}\right) \tag{6.2}$$

For this method, T_e values are binned by using a moving window binning scheme. This is achieved by determining the size of the first bin, the bin intersection length, and lastly the minimum number of observations in a bin. The last step essentially determines when the last bin will occur. All three of these steps require a user-defined parameter that will determine the binning scheme. These parameters will likely affect the final contour generation and consequently, contours need to be evaluated for their sensitivity to these parameters. Each bins lognormal distribution requires 2 parameters that need to be estimated. These are estimated by using a linear model approximation of the relationship between the sample mean and the sample standard deviation of the H_s values in each bin, across each bin.

Based on trends observed in the data, the following relationships are used:

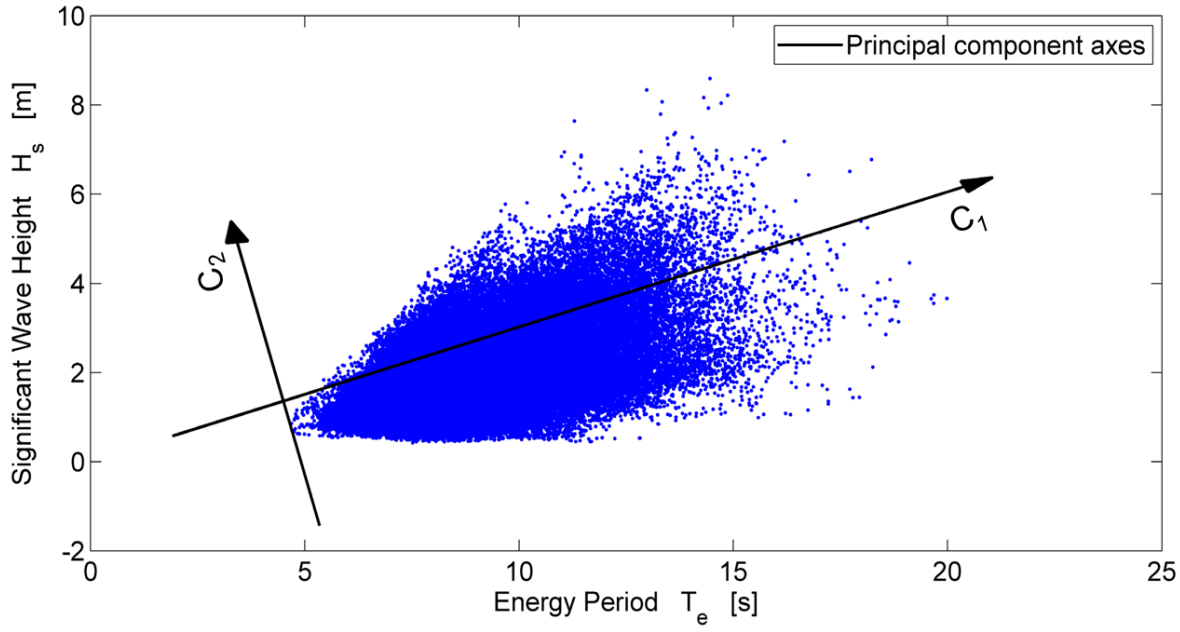

Figure 6.2: C_1 and C_2 become the new axes that remove the correlation between H_s and T_e [1]

$$f_\mu(H_s) = \beta_0 + \beta_1 H_s + \beta_2 H_s^2 + \beta_3 H_s^3 \tag{6.3a}$$

$$f_\sigma(H_s) = \gamma_0 + \gamma_1 H_s + \gamma_2 H_s^2 \tag{6.3b}$$

where β and γ are least square regression coefficients.

PCA Method

The PCA method is similar to the Rosenblatt method but it uses a set of transformed variables rather than H_s and T_e. Prior to any marginal distribution fitting, principle component analysis is applied to the ordered pairs of H_s and T_e in order to rotate the physical space into a new orthogonal basis in which the two new variables will be uncorrelated. This will generate two new variables C_1 and C_2 in which C_1 represents the largest variation in the data after the rotation. This can be seen in Figure 6.2.

After C_1 and C_2 are established, the model fitting process is very similar to the Rosenblatt method; however, the marginal and conditional distribution choices are no longer appropriate for the new transformed variables. First, an Inverse Gaussian is fit to C_1, again through

maximum likelihood estimation:

$$f_{C_1}(x) = \left(\frac{\lambda}{2\pi x^3}\right)^{1/2} \exp\left(\frac{-\lambda(x-\mu)^2}{2\mu^2 x}\right) \tag{6.4}$$

Here, μ and η are the mean and shape parameter, respectively.

Similar to the Rosenblatt method, C_2 values are binned according to their corresponding C_1 values. However, the binning scheme is not the same as above. Here, there is a single parameter that defines a fixed number of observations to constitute each bin with no overlap between them. The benefit to this approach is that there are less parameters to define with the drawback being that a moving window binning scheme could potentially provide a smoother fit.

While both binning schemes could have been used in either method, they are not because of the order in which they were developed in the WDRT. The PCA method was the first method in the toolbox while later methods were added with the potential improvement of a moving window binning scheme. One goal of this study is to investigate how much these different binning schemes will affect the final contour.

Another difference from the Rosenblatt method is the choice of the conditional distribution of C_2 conditioned on C_1. The normal distribution was found to be a better fit with parameters based on the following relationship trends observed in the data:

$$f_\mu(C_1) = \beta_0 + \beta_1 C_1 \tag{6.5a}$$
$$f_\sigma(C_2) = \gamma_0 + \gamma_1 C_2 + \gamma_2 C_2^2 \tag{6.5b}$$

where β and γ are least square regression coefficients.

Copula Methods

The rest of the contour methods evaluated in this study involve the use of copulas to capture the dependency between H_s and T_e. Copulas are functions that use correlation measures of the data in order to characterize the relationship between two marginal distributions and couple them into one joint distribution. A more detailed explanation of copulas and their application to contour generation can be seen in [5].

Rather than fitting a conditional lognormal distribution to T_e as in the above non-copula examples, a lognormal distribution is fit to the T_e values themselves as a marginal distribution. Then a conditional copula is used based on correlation parameters between H_s and T_e. That copula is then used as the conditional distribution in the joint density. The copulas

that are considered in this study are the Gaussian, Gumbel, and Clayton copulas. Their respective conditional copulas can be seen in Table 6.1.

Table 6.1: Copula methods.

Name	Equation		Variables
Gaussian	$C_{T_e\|H_s}(t\|h) = \Phi\left(\frac{\rho(t) - \varrho\rho(h)}{\sqrt{1-\varrho^2}}\right)$	(6.6)	• $\rho(t), \rho(h)$: Transformed values of t and h in the normal space • ϱ: Pearson coefficient between $\rho(t)$ and $\rho(h)$ • Φ: Normal standard distribution function
Gumbel	$C_{T_e\|H_s}(t\|h) = h^{-(1+\theta)}(h^{-\theta} + t^{-\theta} - 1)^{-(1+\frac{1}{\theta})}$	(6.7)	• θ: A parameter related to Kendall's Tau (a correlation measure)
Clayton	$C_{T_e\|H_s}(t\|h) = C(t,h)\frac{[(-\ln h^\theta + (-\ln t)^\theta]^{-1+\frac{1}{\theta}}(-\ln h)^{\theta-1}}{h}$	(6.8)	• θ: A parameter related to Kendall's Tau • $C(t,h)$: The joint distribution of the Clayton Copula, see [5]

6.2.2 I-FORM Process

Now that the marginal and conditional distributions have been fit, they can be used to generate environmental contours using the Inverse First Order Reliability Method (I-FORM) outlined in [41]. The process starts by determining the probability that a given sea state is characterized as an extreme event. Given a return period (t_r) and a measurement interval (t_s), both given in hours, the equation for this probability is

$$p = \frac{1}{365 * \left(\frac{24}{t_s}\right) * t_r}. \tag{6.9}$$

Through the Rosenblatt transform [42], that probability will define a radius β of an isoline in the standard normal space. The value for β is achieved by taking the inverse CDF of the standard normal distribution. In the normal space, the circle generated by β will be ordered pairs (u_1,u_2) of extreme events in the normal space. In practice, this will be a finite number of pairs.

In order to convert these ordered pairs of extreme events back into the physical space, the quantile position (q_1,q_2) is calculated by evaluating the standard normal CDF at the corresponding values of (u_1,u_2). Lastly the resulting quantile values are input into the corresponding inverse CDFs of the marginal distribution of H_s (or C_1) and the conditional distribution of T_e conditioned on H_s (or C_2 conditioned on C_1):

$$\Phi(u_1) \rightarrow F^{-1}_{H_s}(q_1) \tag{6.10a}$$
$$\Phi(u_2) \rightarrow F^{-1}_{T_e|H_s}(q_2) \tag{6.10b}$$

These formulas will generate the ordered pairs of the contours in the physical space in all but the PCA case. In this case the ordered pairs create the contour in the principle component space. In order to convert these points back to the physical space, the points need to be rotated inversely to the rotation that initially transformed them into the principal component space.

After taking into account the above consideration in the PCA case, all of the ordered pairs calculated from this process will generate the contour for the given return period of interest:

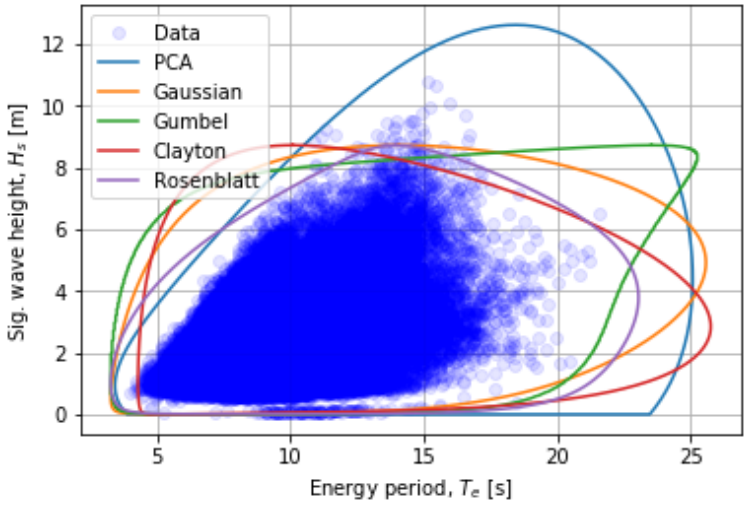

Figure 6.3: Different contour methods produce significantly different shapes for given site data.

6.3 Study Goals

The above contour methods can produce widely varying contour estimates for a given return period. To better understand the performance of these different methods, each of the contours were evaluated on their sensitivity to various parameters, as well as their predictive ability.

6.3.1 Sensitivity

The Rosenblatt and the PCA have a similar model fitting process that involves binning of the conditional variable values (T_e or C_2) based on their corresponding given values (H_s or C_1) and a conditional distribution fit to the T_e/C_2 values based on their respective bin. The primary difference between the two is the number of binning parameters that could potentially affect the final contour. The Rosenblatt method has 3 parameters which will all be tested separately while the PCA method only has one parameter to be tested. Of course, the copula methods will not need to be tested for this since they do not rely on any sort of binning scheme. One of the goals of this study is to see how the final contours are affected by various binning sizes.

In addition, the final contours may be sensitive to the data itself. It is possible that outlier observations can affect the final contour in significant ways. Bootstrap resampling will be used to see how various samples change the final contour.

Another parameter potentially sensitive parameter in contour generation is the return period of interest. How is a 25 year contour different from a 100 year contour? Its expected

that the contour should expand as the return period increases but it is unclear by how much. Understanding the size of the contour as a function of return period could potentially give some insight into trends of expected extreme events.

Lastly, a buoy with irregular observations of H_s and T_e is used as a case study to see how well the contour methods uphold their underlying statistical assumptions in extreme cases. As will be explained later, these extreme cases may not be of practical concern to a WEC engineer. However, it is still interesting to understand potential limitations that may arise with less well-behaved data.

6.3.2 Predictivity

A well performing contour should achieve two things: There should be a minimal amount of points outside of the contour and it should fit the data reasonably well. The first of these points is easier to conceptualize and test. Since one of the underlying assumptions of the model is that the probability of any given sea state being characterized as extreme at a given time is very low. Based off the given p from (6.9), the probability that any number of points are outside of the contour for a given return period can be calculated; as will be seen later, the number of points outside the contour should be fairly low.

It is slightly more difficult to test whether or not a contour fits reasonably well; however, this is an important consideration. If a contour is excessively large then it will be overly-conservative. Overly-conservative estimates of sea states can produce WECs that are too sturdy, too expensive to make, or do not efficiently achieve resonance due to their size/sturdiness. The fit of the contours will be evaluated through a qualitative look at the generated plots, as well as a ratio metric to be explained in more detail in the subsequent sections.

6.4 Methods

All sensitivity and predictivity tests were performed across 4 different sites in varying regions of the United States:

- Buoy 46022: Off the coast of Eureka, CA
- Buoy 46050: Off the coast of Newport, OR
- Buoy 44011: Off the coast of Hyannis, MA
- Buoy 45002: Great Lakes, north of Michigan

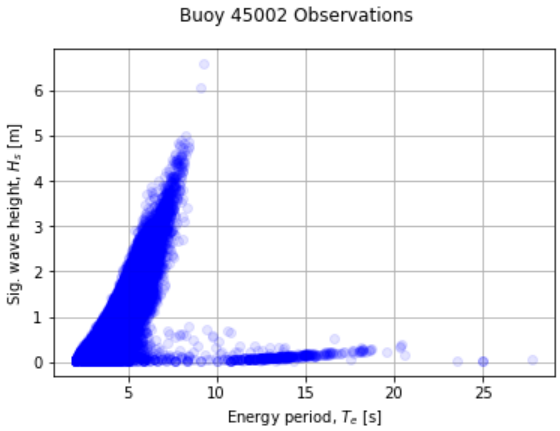

Figure 6.4: The binmodal shape of the data is far different from typical site observation patterns.

6.4.1 Sensitivity

The Rosenblatt contour has 3 binning parameters to test: first bin limit, bin overlap, and minimum overlap. For each parameter, a contour was generated for each of 6 values. The first three values would be relatively small values with a small increment in between them. In order to see how large values would affect the final contour, the final 3 values would have a far larger increment between them. It should be noted that the last value tested was generally chosen to break the contour. For example, a bin overlap of 3 was tested. Since the range of H_s values ranged from 0.12 to 14.07 for a particular site, this would produce 4 bins. Such a low amount of bins loses a lot of information about the dependency between H_s and T_e and would not be optimal. However, it is still important to understand how that affects the final contour. The single binning parameter for the PCA method was tested with 6 values as well with the same logic as above.

In order to test the contour sensitivity to the data itself a bootstrap process of 1000 samples with replacement was taken from a given site. From those samples, a contour was generated for each method. The collection of 1000 contours for each method allowed for the calculation of a 95% confidence interval for each contour method at each location. The idea behind doing this is to take all of the information in the data we currently have, and see how different samples of that data could affect the contour generated. If there is large variation in the possible contours that could be generated from a particular set of data then there would be more uncertainty in the extreme event estimation.

Various return periods were tested to see how it affected each contour. The return periods chosen were: 10, 25, 50, 100, 200 years. The last thing to test with respect to sensitivity of the contours is their sensitivity to irregular buoy data patterns. Buoy 45002 does not have the same cone shape that most locations tend to have. Instead, it has a bimodal shape with one peak of high H_s and low T_e values and another peak of high T_e value and low H_s values:

6.4.2 Predictivity

All of the sites in this study contain at least 20 years of data. In order to assess a contour methods predictive ability, the first 10 years of data for each site was used to generate a contour based on a return period of 25 years. This 25-year contour could then be compared to the actual buoy data gathered over the 20+ years. The contours were evaluated based on how many points are outside of the contour as well as how well the contour fit the realized data.

The number of points outside of the contour was counted (based on optimal parameters discovered in the sensitivity study) for each contour method and each site. As mentioned previously, the probability that a given point is outside of the contour is 6.9. Based on this probability, the probability of the total amount of points outside of the contour can be calculated for the given return period using the binomial distribution:

$$P(X \leq x) = \sum_{i=1}^{n} \frac{n!}{x!(n-x)!} * p^x * (1-p)^{n-x} \tag{6.11a}$$

Here, X is the number of points outside of the contour over the entire return period. Similarly, n is the number of observations in a given return period

Comparing the total amount of points outside of the contour for the 25 year return period to the probability of that occurring will give a strong metric for the contours predictive performance. While the fit of the contour is likely best achieved by comparing the data to the contour in a plot, a metric is given as well. The ratio of the area of the data and the area of the contour was approximated:

$$R = \frac{Area_{data}}{Area_{contour}} \tag{6.12}$$

While it is unclear what an ideal ratio should be between the data and the contour, the ratio will still give a tool for comparing the performance of contours to each other.

6.5 Results

6.5.1 Sensitivity

Binning Parameters

The binning parameters had a far stronger effect on the Rosenblatt contours than they did on the PCA contours. As can be seen in Figure 6.5a, as the size of the minimum bin increases

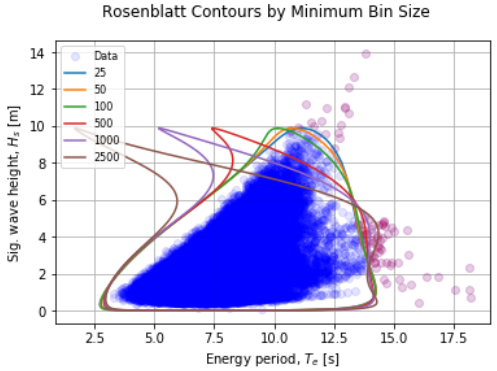

(a) Rosenblatt contours with different bin sizes. As the bin size increases, the contour distorts away from the observations.

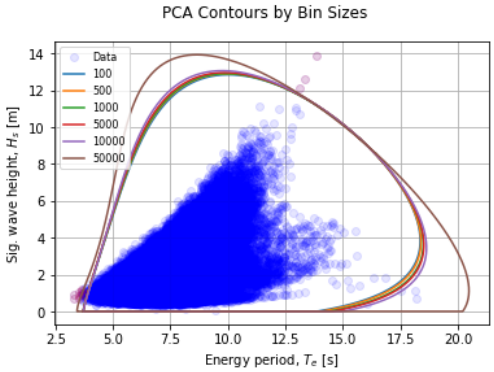

(b) PCA contours with different bin sizes. The contour doesn't change much with respect to binning until they get excessively large.

Figure 6.5: Contour bin size results.

the final contour begins to increase in distortion. This is a strange distortion since the contour is stretching in a direction in which there are no observations. In fact, the binning parameter likely needs to be capped at a reasonable value. If not, the contour can distort to unrealistic sizes (see appendix Figure C.1). The other two binning parameters did not have quite as extreme of an effect as minimum bin size but did change the contour as the sizes changed. Both of these parameters need to be capped at a reasonable value as well. Examples of this can be seen (appendix Figure C.2 and Figure C.3).

The PCA contours were sensitive to the binning parameters but not nearly as much as the Rosenblatt contours. Most choices for the binning parameter produced similar contours. However, this parameter needs to be capped as well. At the most extreme bin choice of 50,000 observations per bin (this would produce 3-4 bins in most cases) the contour began to distort.

It is difficult to assess whether the difference in sensitivities between the two methods is due to the methods themselves or the binning scheme. If, purely based on how the contours are generated with minimal amount of bins, it seems Rosenblatt is more sensitive. However, both binning schemes should be tested on both methods before any conclusions can strongly be drawn.

Buoy Data

While the contours did vary in their sensitivity to the data, none had large variations in the 95% confidence interval. As can be seen in Figure 6.6a, most of the Rosenblatt contour remains unchanged. However, it does change slightly in areas where the data is less dense. Figure 6.6b is typical of the 95% confidence intervals of the copula contours. The 95% confidence interval is much smaller than the non-copula methods even in areas where the

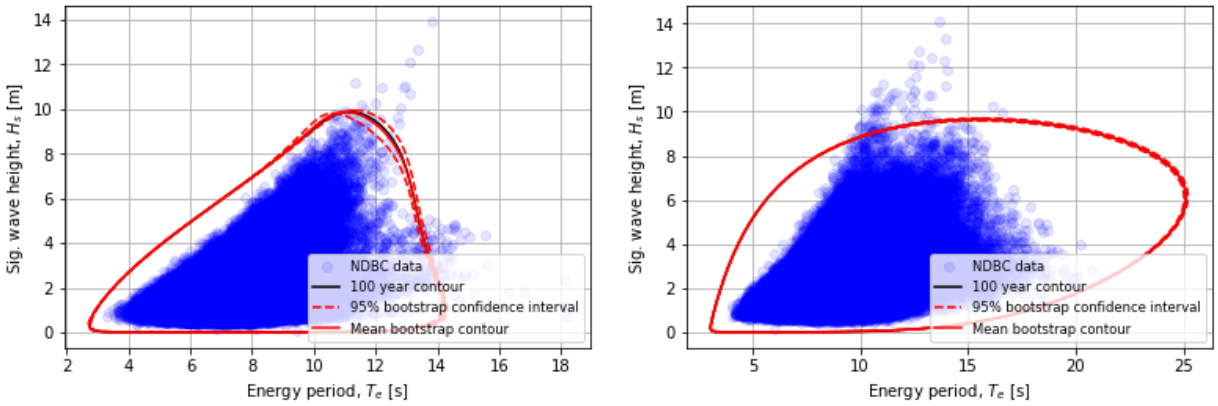

(a) Rosenblatt contour bootstrap. All contours in the 95% confidence interval fit the data well.

(b) Copula contour bootstrap. There is not much change within the 95% confidence interval for the copula methods.

Figure 6.6: Bootstrap contour results.

data is less dense. It seems that none of the copula methods are sensitive to the data whereas the Rosenblatt and PCA methods are slightly sensitive to the data. More examples of copula bootstrap samples as well as the PCA case can be found in the appendix.

Return Period

All of the contours performed similarly with respect to the return period of interest. As expected, as the period increased, the contour would expand as well. This makes sense intuitively as the events that would be characterized as extreme are more likely to occur over a larger interval than a relatively smaller one. One important observation to note (in appendix Figures C.7 and C.8) is that the contour expands more where the data is less dense. This is a good thing since these are the areas where extreme events are more likely to occur. Also of interest is how much the contours expand with respect to the return period. In all cases, the difference between a 10-year and a 25-year contour is larger than the difference between a 100-year and a 200-year contour. This seems odd but does align with the intuition of the tail of the joint distribution. As more extreme cases are examined at the far ends of the tails, the difference in their probabilities is not as great as less extreme parts of the tail.

Odd Buoy Data

While most sites have patterns of data similar to the ones seen above, there are some sites that do not follow these trends and could be a potential problem for the current contour methods. One such site is in Northern Michigan where buoy 45002 resides. As can be seen in Figure 6.8, none of the contour methods seem to adequately capture the bimodal pattern of the data. All of the contours seem to focus on the higher peak while ignoring the second.

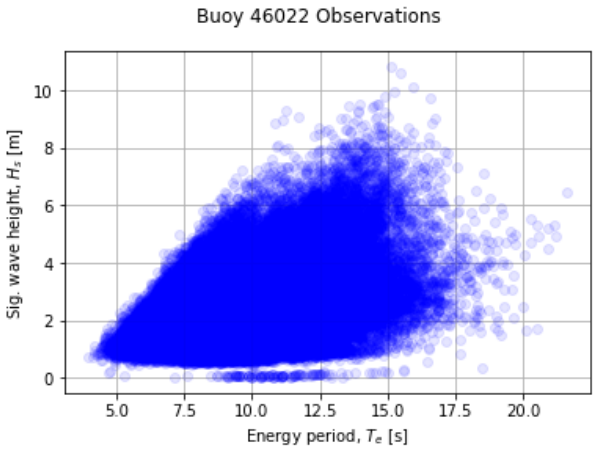

(a) Data shows a cone shape with less dense observation patterns at higher values of H_s and T_e.

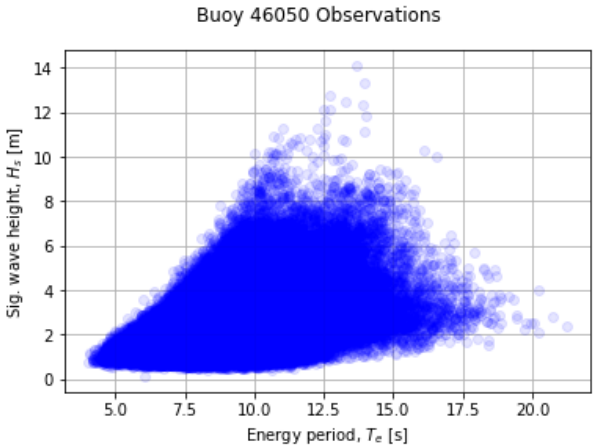

(b) The data has a similar shape to buoy 46022

From a statistical standpoint, this is troublesome as there are far too many extreme observations outside of the contour. However, from a practical standpoint this is not likely a problem. The extreme points that the contours are not capturing are waves with small heights and larger periods, the types of waves that are not likely to damage a WEC. Hence, an engineer will likely be more concerned with the higher mode anyway which is the ones the contours are capturing.

It does seem as though certain contours are better at capturing that second mode than others. The Rosenblatt, Gaussian and Gumbel contours seem to fit the shape nicely while the PCA and the Clayton contours inflate in areas where extreme observations are far less likely based on the trends of the current data.

6.5.2 Predictivity

Based on (6.9) and (6.11) the following probabilities were calculated for each site, where x is the amount of points outside of the contour for the 25-year return period. Figure 6.9 shows that the probability of having 4 or more observations outside of the contour is very unlikely given the models assumptions. As will be seen this is a problem for most of the contours.

Rosenblatt Method

Rosenblatt contours generally have a problem with prediction. For buoy 46022, the contour had 31 points outside of the contour for the 25-year return period which has an extremely low probability of occurring based on the model assumptions. However, the contour does generally provide a good fit to the data. As will be seen in this section 0.61 is one of the better area ratios for a contour. Another benefit to the contour is that its shape is somewhat

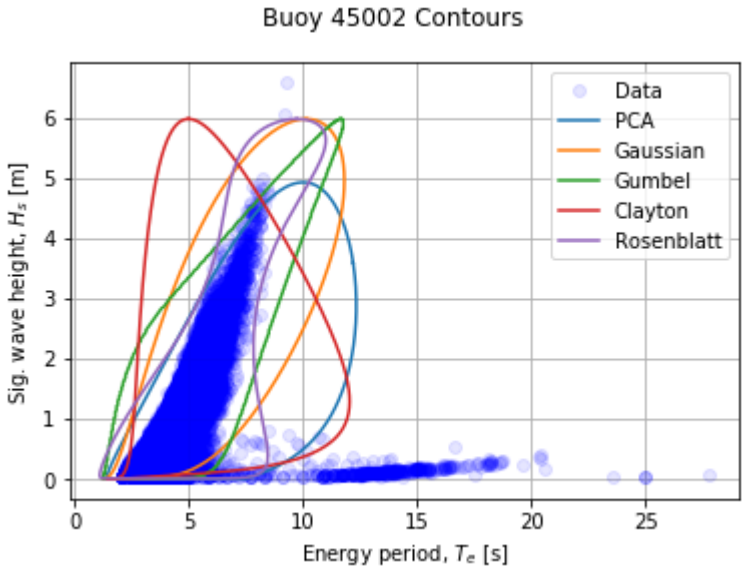

Figure 6.8: No contour method adequately represents both modes of buoy 45002's data distribution.

sensitive to the data in that it changes to fit the shape of the data. As will be seen in the copula methods, this is not always the case.

PCA Method

PCA contours generally did the best with respect to making sure a minimal amount of points at most were outside of the contour. As can be seen from the plot, the price to pay for this is a conservative fit on the right side of the data. As mentioned prior, calculations based off of this could lead to the creation of WECs that are over-designed. The area ratio of 0.39 is one of the lowest values of the study, suggesting that the PCA method might not provide the best fit.

Copula Methods

The copula methods provided an interesting case in prediction. The Gaussian copula generally had the fewest amount of points outside of the contour compared to the others, yet still, the probability of having 29 points outside of the contour is very low given the model assumptions. Again, it should be noted that not all of the points outside of the contour may be of practical concern. Figures 6.12, 6.13, and 6.14 show typical behavior of the Gauss, Gumbel and Clayton contours. In Figure 6.14 for example, many of the outside points are in the bottom left corner. While these waves could be considered statistically extreme, they are hardly physically extreme. Thus, in practice, these outliers are not too concerning.

Buoy	Obs.	$P(X = 0)$	$P(X = 1)$	$P(X = 2)$	$P(X = 3)$	$P(X \geq 4)$
46022	148,003	.51	.34	.12	.03	.0007
46050	160,250	.48	.35	.13	.03	.001
44011	130,575	.55	.33	.1	.02	.0004
45002	98,371	.64	.29	.06	.01	.0001

Figure 6.9: Probability of having n or more observations outside of contour given models assumptions.

The ratio metrics of the copulas were in the mid-range of the contours generally and even though the Gaussian fit the best in this example, this was not necessarily consistently the case; different copula contours fit better depending on the shape of the data.

One concern that is not captured by the ratio metric is that some contours have area where there is no data. As can be seen in Figure 6.13, there is a point in the top right corner of the contour that does not seem to be indicative of the shape of the data at all. In fact, this shape was typical for all of the Gumbel contours generated. A common feature of all of the contour methods is that the shape imposed by the copula did not seem to change that much across sites. The Figure 6.14 shows a shape that is inflated on the left side of the data along where a wave would typically break; this inflation can be seen for most sites in the study. It is concerning because the model is predicting extreme waves that probably are not physically possible.

In general, the copula methods seem to perform at the middle ground between the fit size of the Rosenblatt and the fit size of the PCA. Figures in the appendix show more examples of the rigid shape of the various methods and how that shape did not change much across sites. Because of its more natural shape, the Gaussian Copula generally performed the best of all of the copula methods.

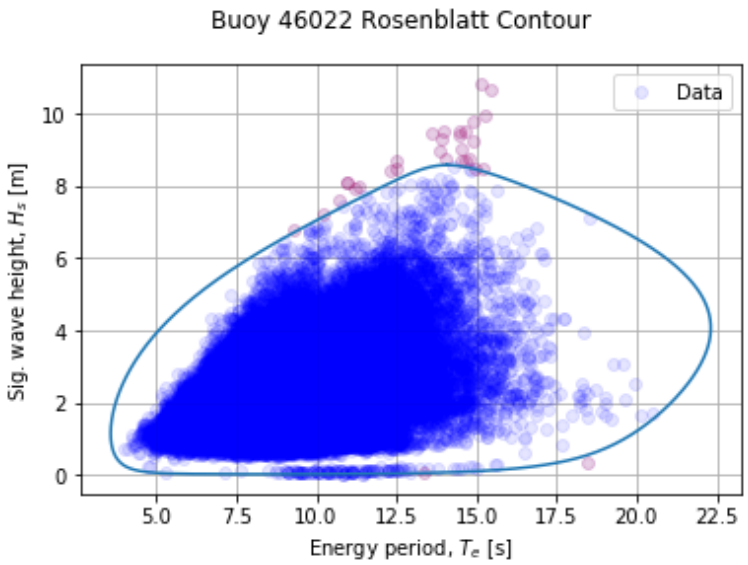

Figure 6.10: The Rosenblatt contour provides a reasonable fit with excessive observations outside of the contour (Outside Points: 31; Area Ratio: 0.61).

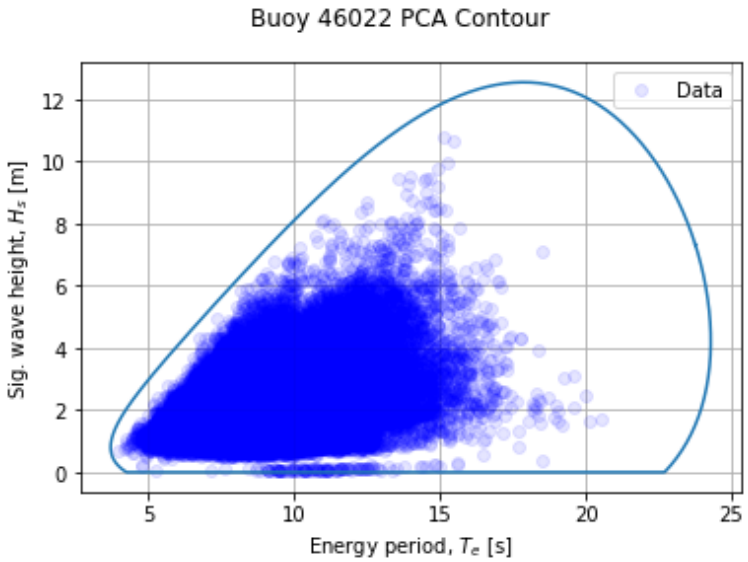

Figure 6.11: The PCA contour provides a conservative fit, however it does keep all observations within the contour (Outside Points: 0; Area Ratio: 0.39).

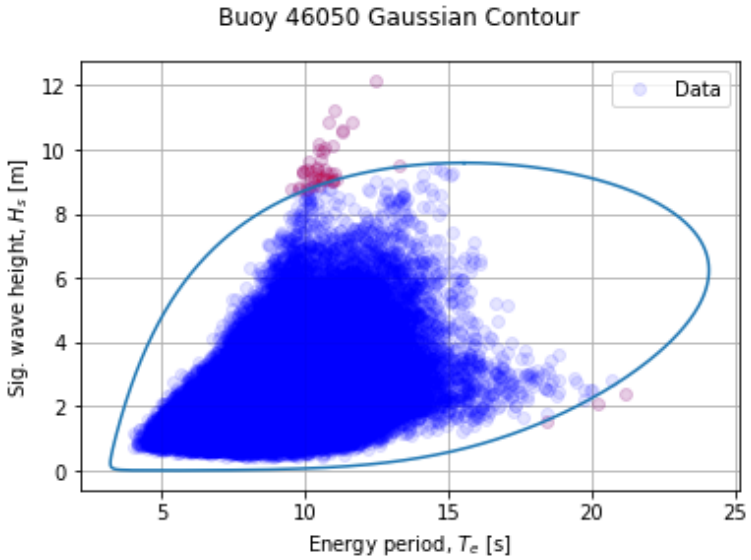

Figure 6.12: The Gaussian contour is excessively conservative on the right side; (Outside Points: 29; Area Ratio: 0.64).

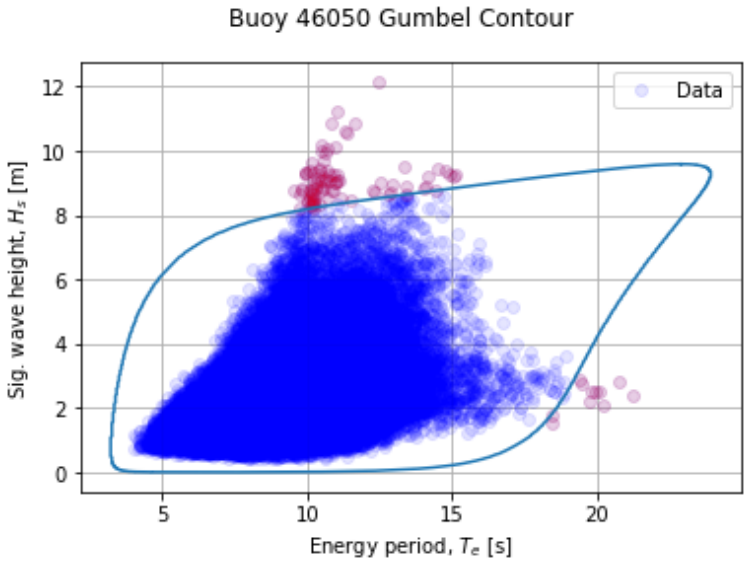

Figure 6.13: The Gumbel contour imposes a pointed shape in the top right that does not appear to be indicative of the data (Outside Points: 96, Area Ratio: 0.57).

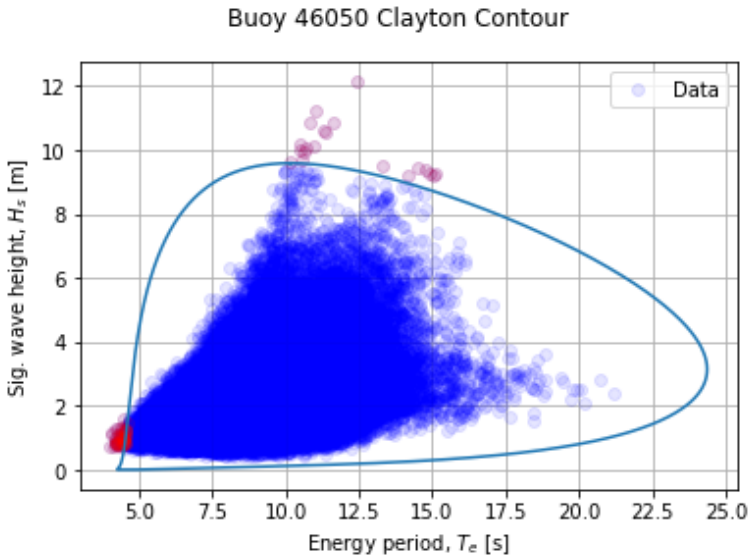

Figure 6.14: The Clayton contour seems to be excessively inflated along the breaking wave line, on the left side of the data (Outside Points: 74; Area Ratio: 0.55).

6.6 Conclusion

The inclusion of multiple contour methods in the WDRT seemed to be justified by this study as no contour performed uniformly better than the others for each site; every method has benefits and drawbacks.

The Rosenblatt and the PCA contours were generally flexible to the shape of the data, with the Rosenblatt usually providing a better fit. The most distinctive drawback to the Rosenblatt was its sensitivity to its binning parameters and the data. While the 95% confidence intervals showed that resampling of a sites observations does not change the contour excessively, changes in the binning parameters had a distinctive effect on the final contour. As the binning parameters created larger bins, the contours distorted to shapes that were no longer representative of the data. It was also found that there was generally an excessive amount of observations outside of the contour in the 25-year prediction study.

With respect to making sure there were a minimal amount of extreme events outside of the contour, PCA usually performed the best. This was the only method in which the results of the 25-year predictive study seemed to align with the models original assumptions about how probable an extreme event should be. The reason why this isnt the uniformly best method is that the trade-off to the above benefit is that it may be a conservative estimate. The area of the contour was quite larger than the area of the data. This might be acceptable for an engineer that wishes to use the environmental contour to build a WEC but they should understand that designs based on this contour could produce WECs that are sturdier (and therefore more expensive) than they need to be.

The copula methods didnt seem to have as much distinctive strengths as the other two non-copula methods. One benefit is that these methods do not rely on any binning structure. Unlike the other two methods, the contour generated will not be affected by any parameters that are not directly derived from the data. In addition, the 95% confidence intervals were noticeably smaller than the other two methods. This implies that copula contours should have generally consistent results. The distinctive drawback to the lack of sensitivity is that the copula often imposed a rigid shape that was not always indicative of the data. That same rigid shape for a given copula would not change much from site to site even if the underlying distribution of the data was different. The final result of that effect is that the methods were generally not that predictive as there was often an excessive amount of observations outside of the contour.

Based on these findings, the PCA method should be generally preferred for environmental contour generation. The estimate for the extreme event contour using this method will likely be conservative and will not underestimate the amount and/or magnitude of extreme events. If an engineer wishes to generate a contour that will not be as conservative, at the risk of underestimating the amount of extreme events, the Rosenblatt contour could be a viable option. As long as a design engineer uses the default binning schemes that were found as a result of this study, they should not be at risk of creating a distorted contour.

References

[1] Aubrey Eckert-Gallup, Cedric J. Sallaberry, Ann R. Dallman, and Vincent S. Neary. Application of principal component analysis (PCA) and improved joint probability distributions to the inverse first-order reliability method (I-FORM) for predicting extreme sea states. *Ocean Engineering*, 112:307–319, 2016.

[2] R.G Coe, V.S. Neary, M.J. Lawson, Y. Yu, and J. Weber. Extreme conditions modeling workshop report. Technical Report NREL/ TP-5000-62305 SNL/ SAND2014-16384R, Sandia National Laboratories and National Renewable Energy Laboratory, 2014.

[3] IEC. Marine energy - wave, tidal and other water current converters - part 2: Design requirements for marine energy systems, August 2016.

[4] S. Haver and S.R. Winterstein. Environmental contour lines: A method for estimating long term extremes by a short term analysis. *Transactions of the Society of Naval Architects and Marine Engineers*, 116:116–127, 2008.

[5] R. Montes-Iturrizaga and E. Heredia-Zavoni. Environmental contours using copulas. *Applied Ocean Research*, 52, 2015.

[6] Gudmund Kleiven and Sverre Haver. Met-ocean contour lines for design; correction for omitted variability in the response process. In *Proceedings of The Fourteenth International Offshore and Polar Engineering Conference*, Toulon, France, 2004.

[7] Made Jaya Muliawan, Zhen Gao, and Torgeir Moan. Application of the contour line method for estimating extreme responses in the mooring lines of a two-body floating wave energy converter. *Journal of Offshore Mechanics and Arctic Engineering*, 135, 2013.

[8] Nianxin Ren, Zhen Gao, Torgeir Moan, and Ling Wan. Long-term performance estimation of the spar-torus-combination (STC) system with different survival modes. *Ocean Engineering*, 108:716–728, 2015.

[9] B.F.M. Child, J. Oberhagemann, M. Hann, D. Greaves, and A. Raby. A methodology for identification and simulation of extreme design load cases for wave energy converters. In *METS2017*, Washington D.C., USA, 2017.

[10] Vincent S Neary, Michael Lawson, Mirko Previsic, Andrea Copping, Kathleen C Hallett, Alison Labonte, Jeff Rieks, Dianne Murray, et al. Methodology for design and economic analysis of marine energy conversion (MEC) technologies. Technical Report SAND2014-9040, Sandia National Laboratories, 2014.

[11] Ryan G. Coe, Carlos Michelen, Aubrey C. Eckert-Gallup, Yi-Hsiang Yu, and Jennifer van Rij. WDRT: A toolbox for extreme response and fatigue analysis of WECs. In *METS2016*, Washington, D.C., 2016.

[12] Y. Yu, K. Ruehl, and C. Michelen. Development and demonstration of the WEC-sim wave energy converter simulation tool. In *2nd Marine Energy Technology Symposium*, Seattle, WA, 2014.

[13] Johannes Falnes. Wave-energy conversion through relative motion between two single-mode oscillating bodies. *Journal of Offshore Mechanics and Arctic Engineering - Transactions of the ASME*, 121(1), 1999.

[14] Ryan G. Coe and Vincent S. Neary. Review of methods for modeling wave energy converter survival in extreme sea states. In *Proceedings of the Second Marine Energy Technology Symposium (METS2014)*, Seattle, WA, 2014.

[15] Chris Chatfield. *The Analysis of Time Series: an Introduction*. Chapman and Hall/CRC, 2003.

[16] Stephen H. Crandall and William D. Mark. *Random Vibrations in Mechanical Systems*. Academic Press Inc., 1963.

[17] A R J M Lloyd. *Seakeeping: Ship Behaviour in Rough Weather*. A R J M Lloyd, 1998.

[18] J. N Newman. *Marine hydrodynamics*. MIT Press, Cambridge, Massachusetts, 1978.

[19] Carlos Michelen and Ryan Coe. Comparison of methods for estimating short-term extreme response of wave energy converters. In *OCEANS 2015 - MTS/IEEE Washington*, Washington D.C., USA, 2015.

[20] Arvid Naess and Torgeir Moan. *Stochastic Dynamics of Marine Structures*. Cambridge University Press, 2013.

[21] R. G. Coe and V. S. Neary. Review of methods for modeling wave energy converter survival in extreme sea states. In *2nd Marine Energy Technology Symposium*, Seattle, WA, 2014.

[22] P. Agarwal and L. Manuel. Simulation of offshore wind turbine response for long-term extreme load prediction. *Engineering Structures*, 31:2236–2246, 2009.

[23] E. Rendon and L. Manuel. Long-term loads for a monopile-supported offshore wind turbine. *Wind Energy*, 17:209–223, 2014.

[24] V. S. Neary, M. Previsic, R. Jepsen, M. J. Lawson, Y. Yu, A. Copping, A. Fontaine, K. Hallett, and D. Murray. Methodology for Design and Economic Analysis of Marine Energy Conversion (MEC) Technologies. Technical report, Sandia National Laboratories and Re Vision Consulting, LLC and National Renwable Energy Laboratory and Pacific Northwest National Laboratory and Pennsylvania State University, Applied Research Laboratory, 2014.

[25] F. G. Giske, B. J. Leira, and O. Øiseth. Long-term extreme response analysis of marine structures using inverse sorm. In *36th International Conference on Ocean, Offshore and Arctic Engineering*, Trondheim, Norway, 2017.

[26] A. C. Eckert-Gallup, C. J. Sallaberry, A. R. Dallman, and V. S. Neary. Modified inverse first order reliability method (I-FORM) for predicting extreme sea states. Technical report, Sandia National Laboratories, 2014.

[27] J. Thomson. Wave breaking dissipation observed with SWIFT drifters. *Journal of Atmospheric and Oceanic Technology*, 29:1866–1882, 2012.

[28] Moored buoy program. `http://www.ndbc.noaa.gov/mooredbuoy.shtml`, 2017. Online; accessed: July-2017.

[29] Measurement descriptions and units. `http://www.ndbc.noaa.gov/measdes.shtml`, 2017. Online; accessed: July-2017.

[30] How are spectral wave data derived from buoy motion measurements? `http://www.ndbc.noaa.gov/wave.shtml`. Online; accessed: July-2017.

[31] J. Talbert J. Thomson and A. de Klerk. Turbulence measurements from moving platforms. *Current, Waves and Turbulence Measurement (CWTM)*, 11:1–5, 2015.

[32] O.M. Faltinsen. Sea loads on ships and offshore structures. In *Cambridge Ocean Technology Series*, 1990.

[33] M. Prat and L. Holthuijsen. Short-term statistics of waves observed in deep water. *Journal of Geophysical Research*, 2010.

[34] Wec-sim (wave energy converter simulator). `http://wec-sim.github.io/WEC-Sim/`, 2015. Online; accessed: July-2017.

[35] S. Lloyd. Least squares quantization in pcm. *IEEE Transactions on Information Theory*, 28:129 – 137, 1982.

[36] D. Arthur. K-means++: The advantages of careful seeding. *Stanford University InfoLab*, 2006.

[37] D. Comaniciu and P. Meer. Mean shift: a robust approach toward feature space analysis. *IEEE Transactions on Pattern Analysis and Machine Intelligence*, 24:603–619, 2002.

[38] K. Fukunaga and L. Hostetler. The estimation of the gradient of a density function, with applications in pattern recognition. *IEEE Transactions on Information Theory*, 21, 1975.

[39] P. J. Rousseeuw. Silhouettes: A graphical aid to the interpretation and validation of cluster analysis. *Journal of Computational and Applied Mathematics*, 20:53–65, 1987.

[40] S. Haver. On the joint distribution of heights and periods of sea waves. *Ocean Engineering*, 14:359–376, 1987.

[41] S. Haver and S.R. Winterstein. Environmental contour lines: A method for estimating long term extremes by a short term analysis. Technical report, 2008.

[42] Murray Rosenblatt. Remarks on a multivariate transformation. *The Annals of Mathematical Statistics*, pages 470–472, 1952.

Appendix A

Computational efficiency

Initially, the WDRT toolbox ran at sufficiently fast speeds in the provided example code. For example, it averaged at 3 minutes for fetching buoy data, processing it, and generating 5 different contors: a Gumbel, a Gaussian, a Clayton, a Rosenblatt, and a PCA contour. This computing speed is decent for analyzing a single buoy. However, for analyzing an entire database, the current rate of calculation implies it would take hours to generate every contour for every buoy. There are a few things that can be done to increase the efficiency of this code.

The WDRT toolbox is written in Python 2.7, which contains a variety of different data structures, such as linked lists, known simply as a *list* in Python, as well as a hash map, which Python calls a *dictionary*. However, these standard-library data structures are non-contiguous in memory, meaning the actual binary codes representing the variables contained within the list are not stored adjacent to each other in physical memory. They are also designed to be used for Python's dynamically typed variable, meaning the type of an object (int, string, etc.) is never explicitly defined and is something Python has to keep track of, contributing to some significant overhead. Both of these factors contribute to lists, and Python in general, being very unoptimized for more complex and time-consuming calculations such as the ones present in the WDRT. This is mostly remedied by a third party library known as *numpy*, which contains a standard C-style *array* data structure that is contiguous in memory, and allows the user to statically type the variables held within, as opposed to the dynamic typing system mentioned earlier.

Lists contain a standard-library *sum* function that returns the total sum of everything contained within the list. However, because *lists* are designed to hold any combination of object-types within Python, including user-defined objects, the *sum* function must implement several safety-features such as constant type-checking to ensure it's actually adding numerical together.

Meanwhile, *arrays* are used exclusively for numerical values such as ints, floats, etc., and are optimized to use the numpy function *np.sum*. Because of the ability to statically-type variables, numpy can assume all the values within an array are numerical and thus does not implement the previously-mentioned type-checking systems that Python's standard library implements. Simply switching every instance of the native *sum* to the numpy *sum* increased the efficiency of the code by 3%.

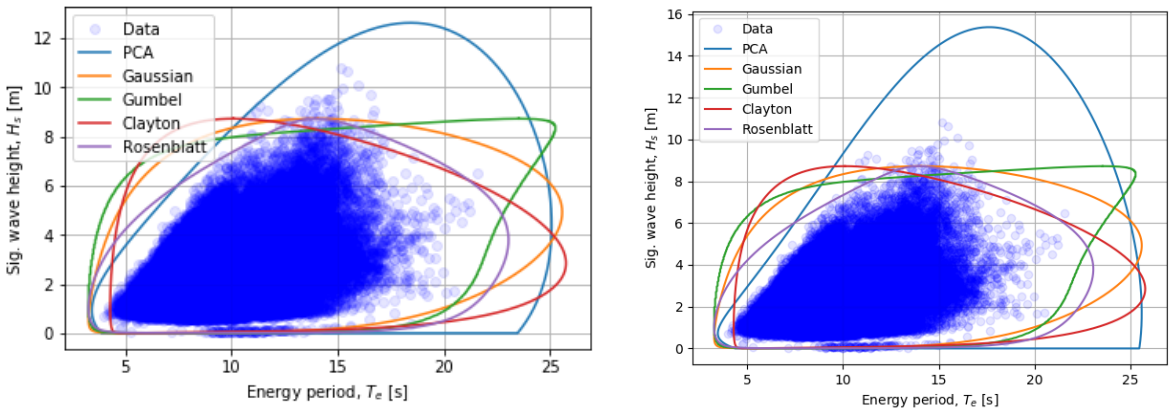

(a) `fmin` (b) `fmin_Powell`

Figure A.1: Comparison between `fmin` and `fmin_Powell` methods.

Additionally, there is an optimization problem in the code concerning non-negative least squares (NNLS). A NNLS problem is one where a mathematical equation or model is fitted to existing data. The end result is an approximation of an equation, which can then be manipulated in other ways, such as taking derivatives or integrals. The WDRT tries to fit the data to the following equation:

$$ax^2 + bx + c$$

where:

$$c \geq 0 \qquad \text{and} \qquad c \geq \frac{b^2}{4a}$$

Because of the nonlinear constraints listed above, this equation is not only quite difficult to solve, in its current form these equations are computationally expensive. Solving this NNLS is currently accomplished by an algorithm that calls upon the `scipy` module. The `scipy` module contains a lot of tools used for fitting functions and minimizing huge problems. However, the `scipy` package is very computationally large in its current state, and as such, the current function for fitting the data is quite computationally expensive.

Scipy does contain approximately 10 different variations on the `fmin` algorithm. When testing each method in the code, 5 of them returned with errors due to needing extra values, such as the gradient, that currently cannot be found. With the remaining methods, all added approximately 15 seconds or more to the runtime, an increase of about 8.3%, enough to negate the previous benefits and more. In addition, they changed the shape of the PCA contour. Figure A.1 is a comparison of the difference between the `fmin` and `fmin_powell` algorithms:

Due to the added runtime and the unintentional data manipulation, we kept the original algorithm, `fmin`.

Appendix B

Data Validation

During the Data-Collection process of the Site Cataloging study, it became evident that a few specific NDBC sites in specific regions were not producing valid environmental contours. This was seemingly due to a notable number of data points that had a suspiciously low significant wave height compared to their energy period. This forced the environmental contours to "skew" in the direction of these data points which impacted their effectiveness at covering more realistic points. This issue is most notably apparent at NDBC site 45004, which falls in the Great Lakes region. Figure B.1 shows this example site.

In order to find the root cause of this issue, we looked at the raw NDBC spectral wave density data used to generate these contours and found a few values that were suspiciously high. NDBC records Spectral Wave Density on an hourly basis, and does so by separating the energy levels at individual frequencies and recording each energy level at each frequency. A comparison between what one would usually expect a normal years worth of spectral wave density data to look like and a corrupted years worth of data is shown in Figure B.2. Note: Each line in the graph represents an hour of data, with each graph containing 8,760 lines, i.e. the number of hours in a year. Figure B.2 shows a comparison between a corrupted and uncorrupted spectral wave dataset.

As can be seen, one can generally expect energy levels at lower frequencies to be close to zero. In the corrupted data, values at the lowest frequency contain some of the highest energy values in the entire hour of data. This is likely just a noise issue in the measurement done by NDBC or some issue with the physical sensors on their devices, but as seen in the contours generated for this site, these errors in measurement can make a drastic difference in the shape and effectiveness of the contour generation.

To remedy this, an optional data-validation technique was implemented within the ESSC module of the WEC Design Response Toolbox (WDRT). Essentially, the total energy is measured for each hour by integrating that hour of energy. The user then sets a specific percentage of that total energy to act as a "validity threshold". If a value in that hour goes above that specified threshold, then the entire hour's worth of data is ignored. For example, if the user sets the threshold to .3, or 30%, and a value in a given hour contains more than 30% of the total energy within that hour, then that hour of data is ignored. This technique works fairly well at detecting and eliminating the corrupted data and allows the ESSC module to produce contours that fit the data of these buoys much better. The results of the data-validation is shown in Figure B.3.

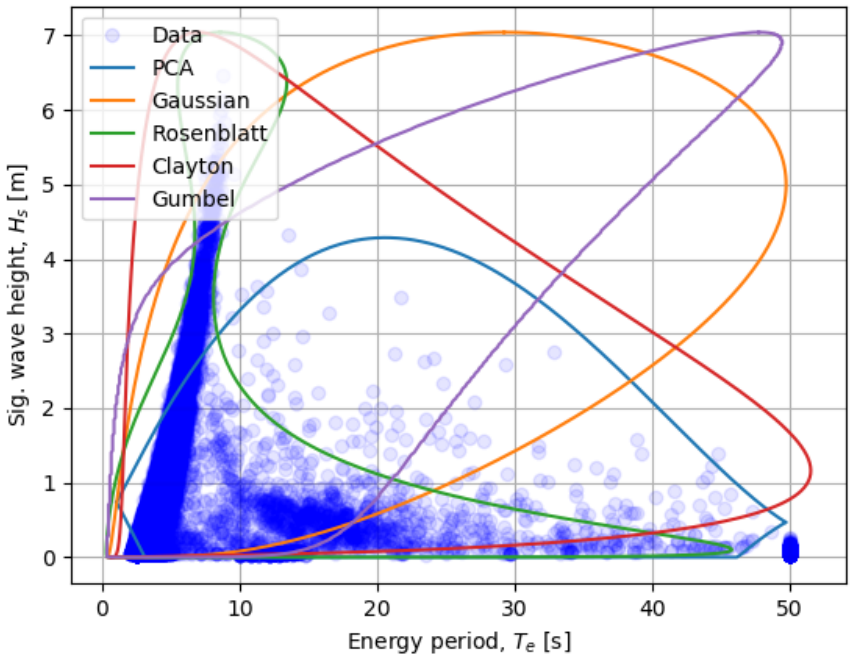

Figure B.1: Environmental contours generated for NDBC45004.

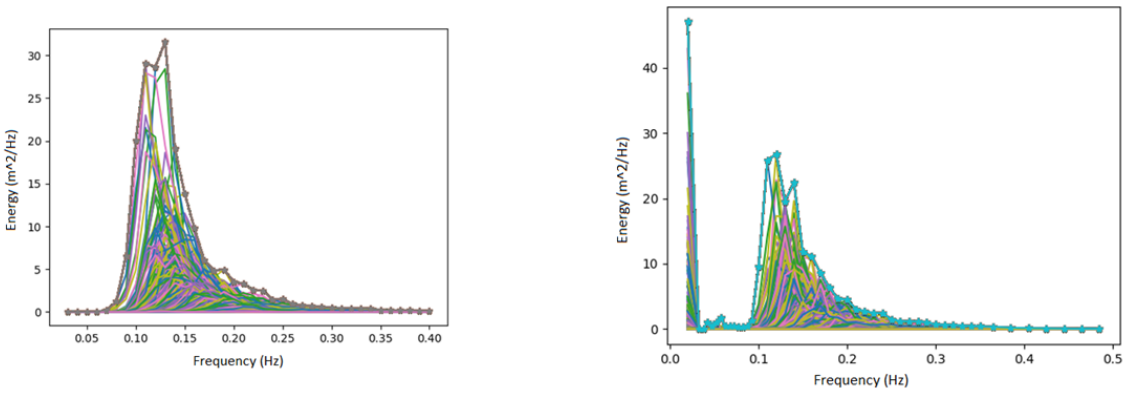

(a) Expected data.

(b) Corrupted data.

Figure B.2: Corrupted and uncorrupted spectral wave data.

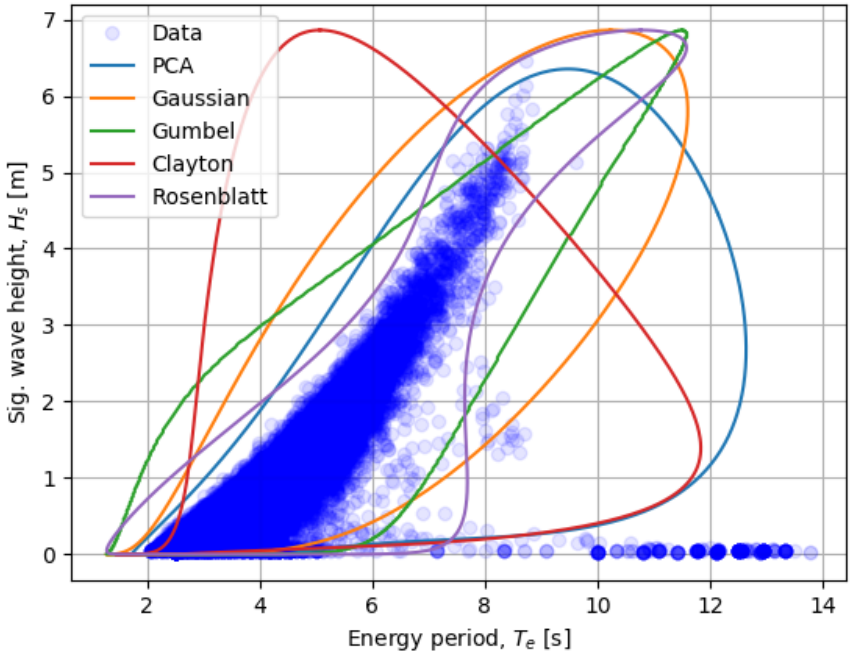

Figure B.3: Environmental contours generated for NDBC45004 after applying the data-validation technique with a validity threshold of 10%

Appendix C

Contour Evaluation

C.1 Binning Sensitivity

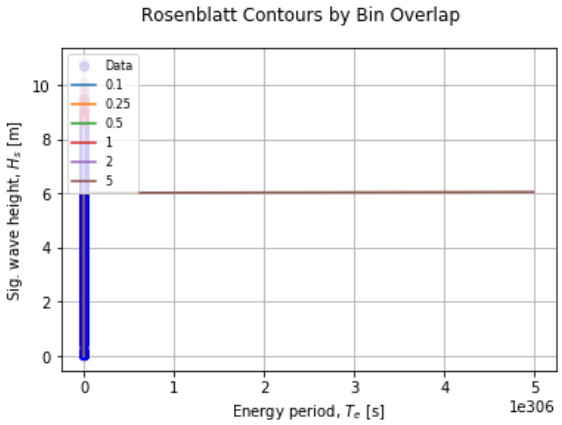

Figure C.1: If bins become too large, the Rosenblatt contour expands to unrealistic lengths.

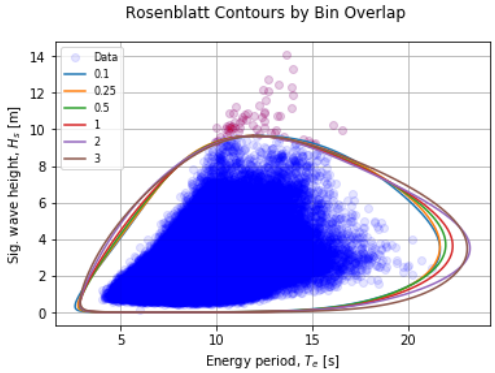

Figure C.2: The Contour is least sensitive to the bin overlap parameter.

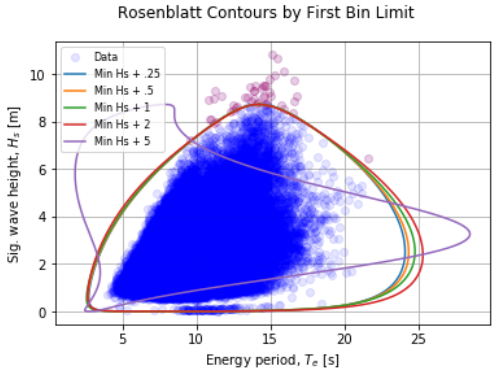

Figure C.3: Most of the bin limits produce similar contours however, excessively large limits will produce a distorted contour.

C.2 Buoy Sensitivity

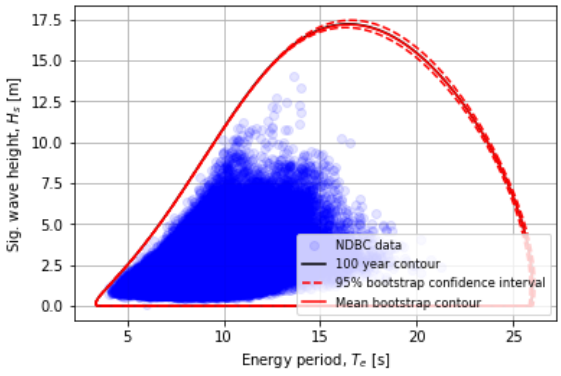

Figure C.4: The 95% confidence interval of the PCA contour generated will still capture all of the observations.

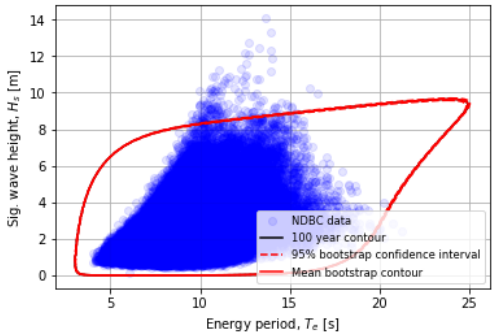

Figure C.5: The 95% confidence interval of the Gumbel contour shows little variation.

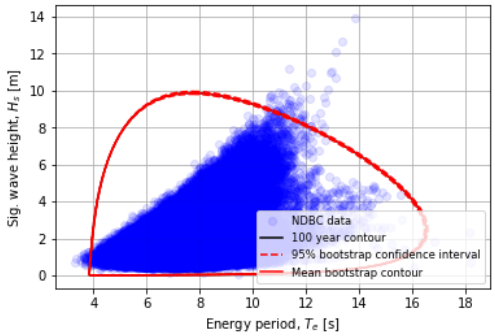

Figure C.6: Many observations are not captured in the 95% confidence interval.

C.3 Return Period

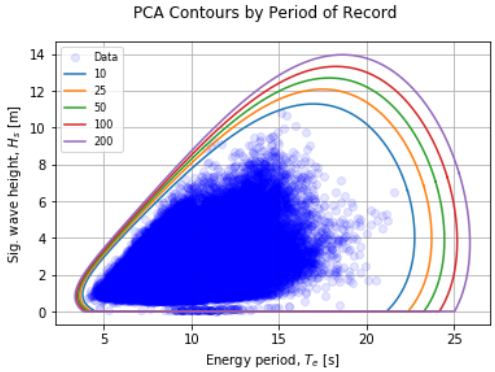

Figure C.7: Like all of the contours, the PCA contour expands where the data is less dense.

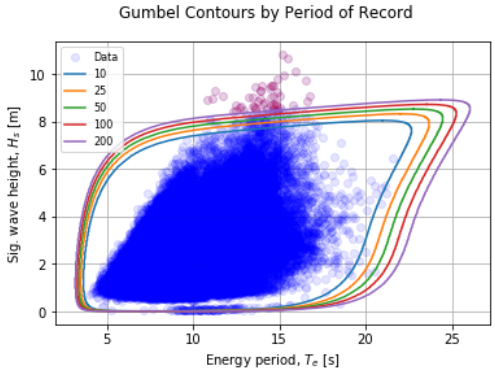

Figure C.8: The contour's shape is retained with each return period.

DISTRIBUTION:

1 MS 0899 Technical Library, 9536 (electronic copy)


Sandia National Laboratories